First-principles study of defects in GaN

Final Report

Period covered: Mar 2008 – Feb 2009

Prepared by

Prof. Dr. Sukit Limpijumnong (P.I.)
and graduate students
Suranaree University of Technology,
Nakhon Ratchasima 30000

sukit@sut.ac.th

For the

AFOSR/AOARD
Contract # FA4869-08-1-4007

Report Documentation Page

Form Approved
OMB No. 0704-0188

1. REPORT DATE **29 JUL 2009**	2. REPORT TYPE **Final**	3. DATES COVERED **01-03-2008 to 01-02-2009**

4. TITLE AND SUBTITLE **First-principles study of defects in GaN**	5a. CONTRACT NUMBER **FA48690814007**
	5b. GRANT NUMBER
	5c. PROGRAM ELEMENT NUMBER
6. AUTHOR(S) **Sukit Limpijumnong**	5d. PROJECT NUMBER
	5e. TASK NUMBER
	5f. WORK UNIT NUMBER
7. PERFORMING ORGANIZATION NAME(S) AND ADDRESS(ES) **National Synchrotron Research Center, Suranaree University of Technology,P.O. Box 93,Nakhon Ratchasima 30000,Thailand,NA,NA**	8. PERFORMING ORGANIZATION REPORT NUMBER **N/A**
9. SPONSORING/MONITORING AGENCY NAME(S) AND ADDRESS(ES) **AOARD, UNIT 45002, APO, AP, 96337-5002**	10. SPONSOR/MONITOR’S ACRONYM(S) **AOARD**
	11. SPONSOR/MONITOR’S REPORT NUMBER(S) **AOARD-084007**

12. DISTRIBUTION/AVAILABILITY STATEMENT
Approved for public release; distribution unlimited

13. SUPPLEMENTARY NOTES

14. ABSTRACT

Based on first principles supercell approach, we have successfully initiated and continued our study of defects in AlN, GaN, diluted nitrides and related wide gap materials. We have also investigated and implemented an approach to calculate the x-ray absorption near edge structures (XANES) by using first principles pseudopotential in conjunction with ab initio multiple scattering codes. We have surpassed our original milestones in several aspects and already accomplished important results. a) We have calculated native defects in AlN, namely VAl, VN, Ali, and Ni. Most of the results are in agreement with previous work by Stampfl and Van de Walle. Except for the Ni, where we have shown that Ni prefers the split-interstitial configuration. b) Potential p-type dopants in AlN, Mg and Be, have been studied. We found that both dopants, when substituting for Al, give a rather deep level. This means both Mg and Be are not suitable p-type dopants in AlN. c) We have calculated the Ga Frenkel pairs (interstitial Ga and gallium vacancy complexes) in GaN. We studied both the stability of the pair at different separations and the barriers for the pair to form/disintegrate. Our results show that the pair at ~ 4 ?separation is stable and has a binding energy of about 3.3 eV. However, the barrier for the pair to recombine is only ~ 0.2 eV, making it unlikely to be stable at room temperature. d) In dilute nitrides, the nitrogen atoms are highly strained. Our calculations show that they prefer to bind with small impurity atoms such as C or Si in the form of CN and SiN molecule, substituting on the As site. The CNAs gives a vibration frequency in good agreement with the local vibration mode observed in an infrared spectroscopy measurement. The SiNAs has low formation energy and could explain the mutual passivation of shallow donor Si and isovalent N in dilute nitride. e) We investigated the local structure of indium oxynitride at various O:N ratios using combined experimental x-ray absorption spectroscopy and first principles calculations. Our results showed that O can substitute on the N site of wurtzite InN upto about 40% then the alloy started to have mixed wurtzite and bixbyite (In2O3 natural structure) phases. The simulated x-ray absorption spectra based on the proposed models are in a very good agreement with the measurements. f) We have revisited the problem of the H binding site in ZnO. In some commercial samples, the vibration frequency of the H atoms indicates that they are binding with O at the bond center site whereas in some samples the frequency indicates that they are at the anti-bonding site. Based on first principles calculations, we showed that Ca, found only in some samples, plays a pivotal role in switching the H from the bond-center site to the anti-bonding site.

15. SUBJECT TERMS					
16. SECURITY CLASSIFICATION OF:			17. LIMITATION OF ABSTRACT	18. NUMBER OF PAGES	19a. NAME OF RESPONSIBLE PERSON
a. REPORT	b. ABSTRACT	c. THIS PAGE	**Same as Report (SAR)**	**48**	
unclassified	**unclassified**	**unclassified**			

Executive summary

Based on first principles supercell approach, we have successfully initiated and continued our study of defects in AlN, GaN, diluted nitrides and related wide gap materials. We have also investigated and implemented an approach to calculate the x-ray absorption near edge structures (XANES) by using first principles pseudopotential in conjunction with ab initio multiple scattering codes. We have surpassed our original milestones in several aspects and already accomplished important results. a) We have calculated native defects in AlN, namely V_{Al}, V_{N}, Al_i, and N_i. Most of the results are in agreement with previous work by Stampfl and Van de Walle. Except for the N_i, where we have shown that N_i prefers the split-interstitial configuration. b) Potential *p*-type dopants in AlN, Mg and Be, have been studied. We found that both dopants, when substituting for Al, give a rather deep level. This means both Mg and Be are not suitable *p*-type dopants in AlN. c) We have calculated the Ga Frenkel pairs (interstitial Ga and gallium vacancy complexes) in GaN. We studied both the stability of the pair at different separations and the barriers for the pair to form/disintegrate. Our results show that the pair at ~ 4 Å separation is stable and has a binding energy of about 3.3 eV. However, the barrier for the pair to recombine is only ~ 0.2 eV, making it unlikely to be stable at room temperature. d) In dilute nitrides, the nitrogen atoms are highly strained. Our calculations show that they prefer to bind with small impurity atoms such as C or Si in the form of CN and SiN molecule, substituting on the As site. The $\mathrm{CN}_{\mathrm{As}}$ gives a vibration frequency in good agreement with the local vibration mode observed in an infrared spectroscopy measurement. The $\mathrm{SiN}_{\mathrm{As}}$ has low formation energy and could explain the mutual passivation of shallow donor Si and isovalent N in dilute nitride. e) We investigated the local structure of indium oxynitride at various O:N ratios using combined experimental x-ray absorption spectroscopy and first principles calculations. Our results showed that O can substitute on the N site of wurtzite InN upto about 40% then the alloy started to have mixed wurtzite and bixbyite ($\mathrm{In_2O_3}$ natural structure) phases. The simulated x-ray absorption spectra based on the proposed models are in a very good agreement with the measurements. f) We have revisited the problem of the H binding site in ZnO. In some commercial samples, the vibration frequency of the H atoms indicates that they are binding with O at the bond center site whereas in some samples the frequency indicates that they are at the anti-bonding site. Based on first principles calculations, we showed that Ca, found only in some samples, plays a pivotal role in switching the H from the bond-center site to the anti-bonding site.

Publications:

1) "*Local structure of indium oxynitride from x-ray absorption spectroscopy*"
   J. T-Thienprasert, J. Nukeaw, A. Sungthong, S. Porntheeraphat, S. Singkarat, D. Onkaw, S. Rujirawat, and S. Limpijumnong
   Appl. Phys. Lett. **93**, 051903 (2008).
2) "*Carbon-nitrogen molecules in GaAs and GaP*"
   Sukit Limpijumnong, P. Reunchan, A. Janotti, and C.G. Van de Walle
   Phys. Rev. B **77**, 195209 (2008).
3) "*Hydrogen in ZnO revisited: Bond center versus antibonding site*"
   X.-B. Li, Sukit Limpijumnong*, W.Q. Tian, H.-B. Sun, and S.B. Zhang
   Phys. Rev. B **78**, 113203 (2008).
4) "*An unexpected Coulomb binding between* Ca *and* H^+ *in* ZnO"
   X.-B. Li, Sukit Limpijumnong, W.Q. Tian, and S.B. Zhang
   J. Vac. Sci. Technol. B **27**, 1601 (2009).

(Following work schedule and milestones are the same as previously submitted)

Work schedule:

Month 0:

- Start calculations of common native defects and dopants (such as Mg and Be) in AlN, focusing on the *p*-type aspects using first principles ultrasoft pseudopotential (USPP) and a supercell approach. Since both Mg and Be are theoretically reported to be good *p*-type dopants in GaN, they are good candidates for AlN and GaAlN alloys.
- Calculations of some impurities in diluted nitrides (such as C-N complexes and Si-N complexes in GaAsN) using first principles supercell approach.

Month 6:

- Low energy native defects in AlN and the potential dopants for *p*-type AlN will be further investigated. Their properties in AlGaN alloys will be studied.
- Start calculations of Frenkel pairs in GaN by first principles supercell approach. The stability of the pairs will be investigated by varying the pair distance. *If needed*, effects of band gap corrections might be investigated by using LDA+*U* approach.
- Simulating the signatures of interesting defects in comparison with available measurements (such as XAS, XPS, PL, DLTS, EPR, or IR spectroscopy).

Milestones:

6 month:

- Obtained the results of at least four native defects (and/or impurities) in AlN.
- Obtained some stable impurity structures and their properties (such as vibration signatures) in diluted nitrides. For examples, CN complexes in GaAsN and SiN complexes in GaAsN.

12 month:

- Complete results on simple native defects as well as Mg- and Be-doped AlN.
- Obtained the binding energies and other properties of the $\mathrm{Ga_i} - V_{\mathrm{Ga}}$ and $\mathrm{N_i} - V_{\mathrm{N}}$ Frenkel pairs in GaN.
- Results on the binding energies and stabilities of Frenkel pairs as a function of the pair-distance.
- Signatures (that can be compared with experimental measurements) of some interesting defects and dopants in AlN (and AlGaN alloys).
- Implications of some interesting AlN defects when formed in AlGaN alloys.

Research Activities

Computational codes

First-principles calculation approach based on density-functional theory and *ab initio* ultrasoft pseudopotentials (USPP) is the main approach for this work. We used the codes called Vienna Ab-initio Simulation Package (VASP) [1]. For the x-ray absorption spectroscopy (XAS) simulation, we use the ab initio multiple scattering code called FEFF (version 8.2) [2]. Note that before calculating the XAS, the accurate atomic relaxations are performed using the first principles USPP codes (VASP). The detail of the parameters and approximations used in the calculations is slightly varied, depending on specific material. Further specific computational detail for each system under study can be found in each attached publications.

A brief description of the defect theory

Calculations for defects in semiconductor are calculated using a supercell containing 32 to 96 atoms and a set of non-Γ k-points sampling.

In supercell calculations, the formation energy of a defect X in charge state q is

$$E_f[X^q] = E_{tot,SC}(X^q) - E_{tot,SC}(bulk) + n_\alpha \mu_\alpha + qE_F \,, \qquad [1]$$

where $E_{tot,SC}(X^q)$ is the total energy of a supercell containing the defect, $E_{tot,SC}(bulk)$ is the total energy of the same supercell but without any defect. n_α is the number of the atoms of specie α being removed from (positive value) or added to (negative value) a bulk supercell to form defect X. μ_α is the reservoir energy of specie α (the chemical potential). E_F is the Fermi level, referenced to the valence-band maximum of bulk, E_v.

The chemical potentials in Eq. [1] depend on the growth conditions. For example, (in the case of defects in AlN) under Al-rich case, μ_{Al} = formation energy of solid metal Al. In order for AlN to be stable during the growth, we also require that $\mu_{\mathrm{Al}} + \mu_{\mathrm{N}} = \mu_{\mathrm{AlN}}$ = constant Φ. This fixes $\mu_{\mathrm{N}} = \Phi - \mu_{\mathrm{Al}}$. The chemical potential of other elements are referenced to their natural phase. For example the chemical potential of C, μ_{C} is referenced to the diamond limit, i.e. $\mu_{\mathrm{C}} = E_{\mathrm{tot}}(\mathrm{diamond})/2$. The total energy of diamond is divided by two because there are two carbon atoms per a diamond unit cell.

Native defects in AlN

We followed the computational approach that we previously used to study defects in GaN [3] and TiO_2 [4] to study native defects in AlN. Test calculations show that using the supercell size of 36 or 96 atoms result in similar formation energy; indicating that 96-atom supercell is sufficiently large for the defect calculations of wurtzite AlN. This is similar to the case of wurtzite GaN. Native defects in AlN have been previously studied by Stampfl and Van de Walle [5] using the pseudopotential planewave method. Their calculations use mainly a 32-atom zincblende supercell except some calculations using the wurtzite supercell or 96-atom wurtzite supercell for convergence tests. Here we use slightly different computational approach (USPP planewave); allowing the calculations with larger wurtzite supercell (all calculations are done with 96-atom cell). Most of the results are in a reasonable agreement with the previous work by Stampfl and Van de Walle [5] with some exceptions as will be discussed below.

1) Vacancies (aluminum and nitrogen vacancies, V_{Al} and V_N)

Similar to many semiconductors, vacancies are the low energy defects in AlN. As shown in Fig.1, under Al-rich conditions, it is more difficult to create aluminum vacancy (V_{Al}); leading to higher energy of V_{Al}. Since, under that condition, nitrogen is scarce, the nitrogen vacancies can be created easily; leading to low V_N energy. Under N-rich conditions, the formation energy of V_{Al} shifted down and V_N shifted up. For V_{Al}, the possible charge states varied from neutral near the VBM to 3- at higher Fermi energy above 1.5 eV (The charge state can be determined from the slope of the plot.) As a result, V_{Al} can be considered as a very deep acceptor that can accept up to three electrons. For V_N, there are two possible charge states, the 3+ charge state at the Fermi energies near the VBM and the 1+ charge state for the higher Fermi energies. The sharp drop in formation energy at Fermi energy above 3.5 eV is an artifact in the calculations from the occupations of the calculated conduction band minimum that have to be ignored. This issue has also been discussed in Ref. [5]. (In the calculations, the band gap appears too small due to the well-known DFT gap underestimation.) In reality the 1+ charge state would extended along the dotted line all the way to the CBM. As a result, V_N is an active donor that can donate three electrons when the Fermi energy is near the VBM (i.e., when the sample is *p*-type) or donate one electron when the Fermi energy lies in the range from 1 eV to the bottom of CBM (*n*-type condition). These vacancy defects could play important roles in compensating the dopants. For *p*-type doping, V_N, as a triple donor, would play an important role in compensating the acceptor dopants. To avoid such compensation, one should perform *p*-type doping under N-rich conditions where the formation energy of V_N is the highest. On the other hand, for *n*-type doping, V_{Al}, as a triple acceptor, would play an important role in compensating the donor dopants. However, V_{Al} is only active under n-type conditions. By itself V_{Al} does not act as an acceptor because the ε(0/−) is very deep, i.e. the defect level is far away from the VBM. This is in contrast to V_N which always act as a donor regardless of the Fermi level of the sample

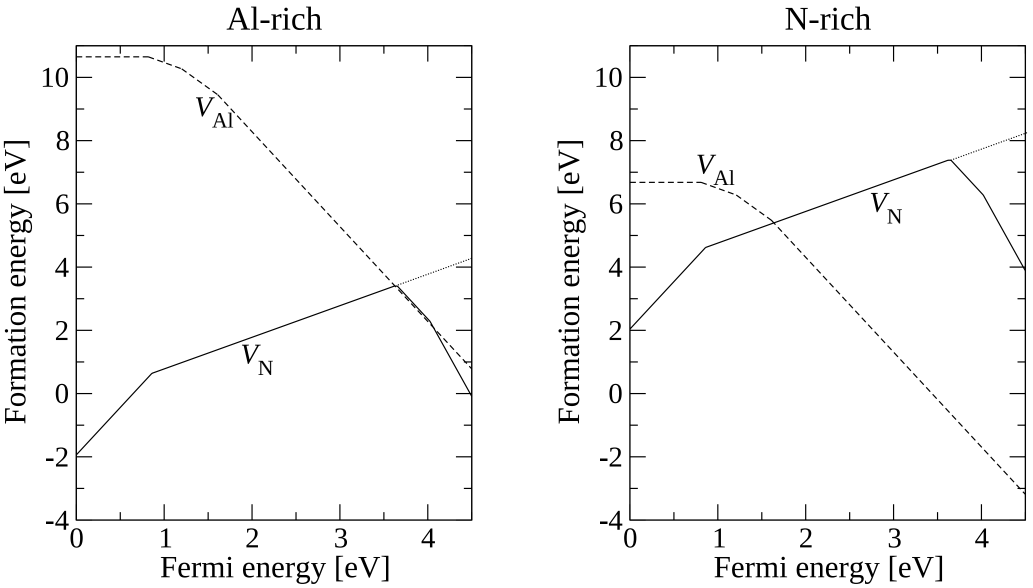

Figure 1: Calculated formation energy as a function of the Fermi level for vacancy defects under the Al-rich (left) and N-rich (right) limits. The Fermi level is references to the top of the AlN VBM.

2) Interstitials (interstitial aluminum and nitrogen, Al_{int} *and* N_{int}*)*

Interstitial defects are generally high in energy than vacancy defects, especially for covalent materials. However, in ionic materials the charged interstitial defects can have low formation energies due to the columbic energy gain between the cation-anion bindings. For example, interstitial titanium in 4+ charge state has been found to have low formation energy in TiO_2 [4]. Here, we found that Al_{int} in 3+ charge state has low formation energy in AlN under Al-rich conditions. From the formation energy plot in Fig. 2, Al_{int} is stable in 3+ charge state for all Fermi energy; indicating that it is exclusively a donor. Note that, the drop in formation energy near CBM is an artifact in the calculations from the occupations of the calculated conduction band minimum that have to be ignored. Interstitial nitrogen in AlN is stable in the split interstitial form which can be viewed as a nitrogen molecule substituting the N site [3, 6]. N_{int} in this form is lower in energy than an isolated form by at least 2 eV. Since Stampfl and Van de Walle [5] did not investigate N_{int} in this form, their formation energy of this defect appears higher. Regarding the charge state, N_{int} is amphoteric defect, i.e. can behave as both donor and acceptor to compensate for the leading carrier in the sample. However, it has reasonably low energy only under N-rich conditions and Fermi energy near the CBM.

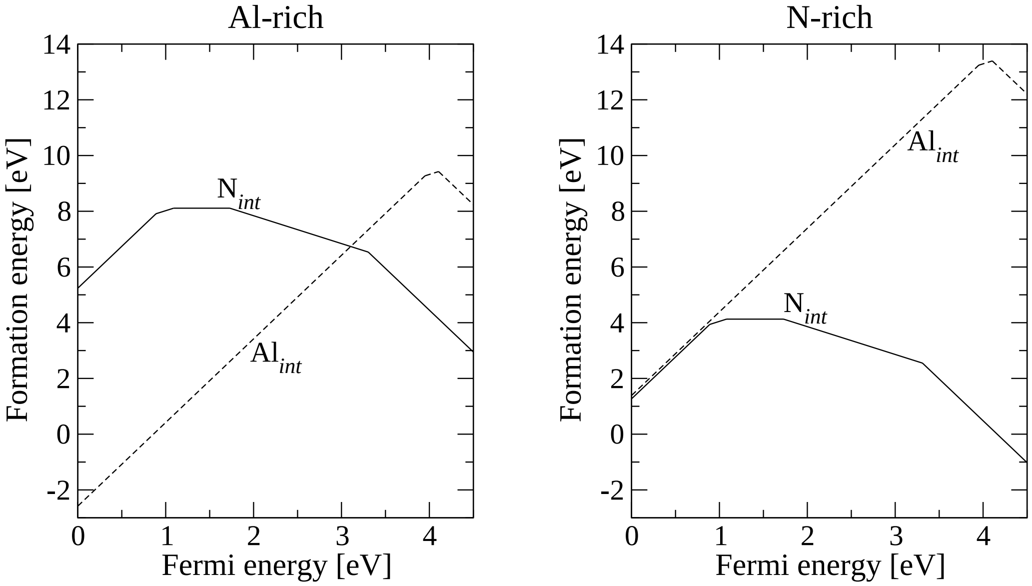

Figure 2: Calculated formation energy as a function of the Fermi level for intersitial defects under the Al-rich (left) and N-rich (right) limits. The Fermi level is references to the top of the AlN VBM.

3) Antisites (aluminum and nitrogen antisites, Al_N *and* N_{Al}*)*

Generally antisite defects have high formation energy, especially in ionic materials. For AlN, which is rather ionic, the antisite defects are reported to be higher in energy than vacancy defects [5]. However, AlN has rather large heat of formation. Our calculated value of ΔH = 3.6 eV is consistent with Ref. [5] of 3.5 eV. This gives a wide variation of (theoretical) possible growth conditions from Al-rich to N-rich. For vacancy defects, this means the variation in formation energy of 3.59 eV from Al-rich to N-rich. However, for antisite defects, this means the variation of 3.6 x 2 = 7.2 eV. As a result, the calculated formation energies of these antisite defects suggested that under extreme Al-rich and N-rich conditions they can be stable. As shown in Fig. 3, the Al_N could be stable in 4+ charge state under Al-rich and *p*-type conditions whereas the N_{Al} could be stable in 4– charge state under N-rich and *n*-type conditions. Our calculations show that these two highly charged antisite defects can be stable over other native defects for a small range of Fermi energy under these two extreme Al-rich and N-rich conditions. This is slightly different from Stampfl and Van de Walle results [5] that found the antisite defects slightly higher in energy than other native defects and have never been the lowest energy defects in any conditions. This is due partly to the fact that our calculated heat of formation is slightly higher than theirs; allowing our extreme Al-rich and N-rich conditions to extend a little bit wider.

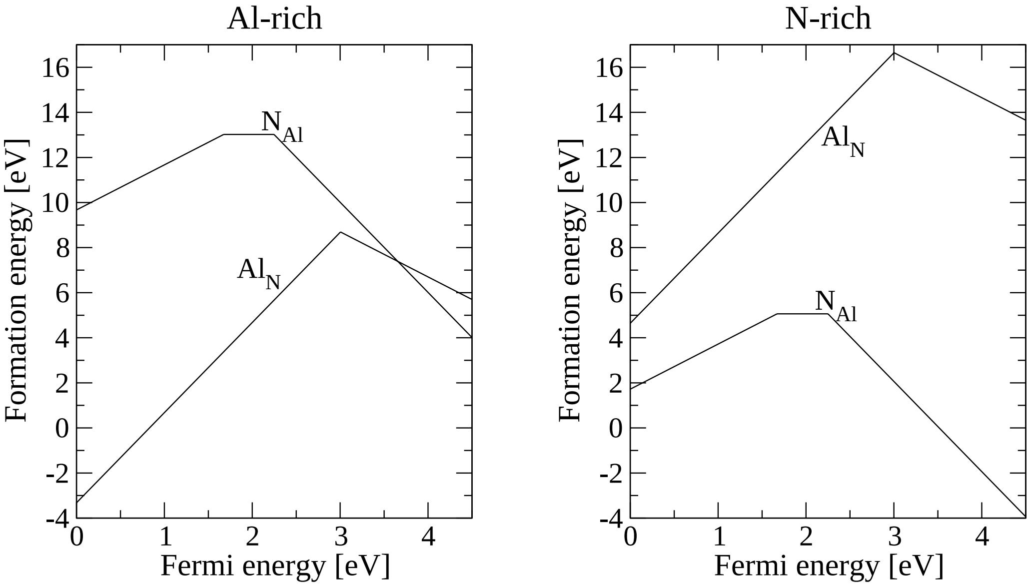

Figure 3: Calculated formation energy as a function of the Fermi level for antisite defects under the Al-rich (left) and N-rich (right) limits. The Fermi level is references to the top of the AlN VBM.

Magnesium and beryllium doped AlN

Magnesium has been used successfully to dope GaN into *p*-type; leading to commercial blue lasers in today devices. We have previously suggested that beryllium is a potentially good *p*-type dopant in GaN as well [7]. However, beryllium can potentially form interstitial (Be_{int}) which is a double donor. Moreover the interstitial is also likely to bind with the substitutional acceptor (Be_{Ga}) turning the acceptor into a single donor. In our previous work [7], we suggested that if one can overcome interstitial Be problem, beryllium is a potentially better acceptor than Mg. Because the lattice constant of AlN is very similar to that of GaN, both Mg and Be are potential candidates as the *p*-type dopants in AlN. However, experiment results show that Mg is a deep acceptor in AlN (with ionization energy of around 0.4 – 0.6 eV)[8]. Here, we systematically study both Mg and Be as dopants in AlN. Interstitial Mg and Be (Mg_{int} and Be_{int}) are also study to access the likelihood that they can cause spontaneous compensation.

1) Magnesium substituting for Al and magnesium interstitial (Mg_{Al} *and* Mg_{int}*).*

Figure 4 shows the formation energies of Mg substituting for Al and interstitial Mg in AlN. It is similar to the case of Mg in GaN that the Mg interstitial always a double donor, i.e. exist only in charge state 2+ regardless of Fermi level. Here the formation energy of Mg_{int} under Al-rich and N-rich are different because the chemical potential of Mg is calculated differently for each case. (If the chemical potential of magnesium is calculated from Mg metal the formation energy of Mg_{int} would not depend on whether the condition is Al-rich or N-rich.) For Al-rich conditions, the chemical potential of Mg is limited to the formation of (fcc) Mg metal. However, for N-rich conditions, it is the Mg_3N_2 formation that precipitates Mg chemical potential. As a result, the formation energy of Mg_{int} under Al-rich condition is slightly lower due to the higher possible Mg chemical potential. For the substitution Mg, obviously the N-rich condition provides the best opportunity for Mg to substitute for Al. Therefore, the formation energy of Mg_{Al} is lower for N-rich condition. According to our calculations, Mg_{Al} is a rather deep acceptor with the ionization energy of 0.69 eV. Under Al-rich condition, Mg_{int} has rather low formation energy and can compensate the Mg_{Al} if there is no other lower energy donor. This suggests that it is difficult to dope Mg into AlN without forming an equal amount of compensating Mg$_{int}$ under Al-rich conditions. However, one might success in doping Mg under N-rich conditions where the Mg$_{int}$ has higher formation energy. Nevertheless, Mg$_{A}$

temp

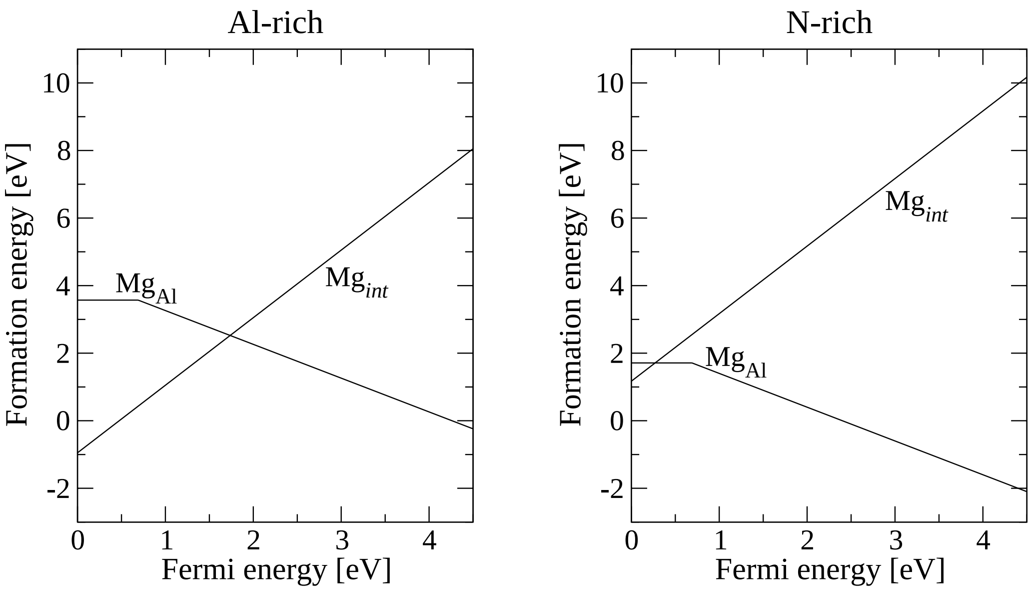

Figure 4: Calculated formation energy as a function of the Fermi level for Mg$_{Al}$ and Mg$_{int}$ under the Al-rich (left) and N-rich (right) limits. The Fermi level is references to the top of the AlN VBM.

*2) Beryllium substituting for Al and beryllium interstitial (*Be$_{Al}$ *and* Be$_{int}$*).*

The formation energies of Be substituting for Al and interstitial Be in AlN is similar to the cases of Mg in AlN shown in the previous paragraph. The Be interstitial is also a double donor. (The neutral charge near the top of CBM is probably an artifact in the calculation caused by the underestimation of the band gap which leads to the wrong occupation.) Figure 5 shows the formation energy of Be$_{Al}$ and Be$_{int}$ in the same fashion as Fig. 4 which is the case of Mg. For Al-rich conditions, the chemical potential of Be is limited to the formation of (fcc) Be metal. However, for N-rich conditions, it is the Be_3N_2 formation that precipitates Be chemical potential. In comparison with the case of Mg in AlN, the formation energy of interstitial Be is much lower than that of Mg$_{int}$. This suggests that Be$_{int}$ can form much easier than Mg$_{int}$ which would cause more compensating problems in AlN. Note that, Be interstitial is also predicted to cause more compensating problem than Mg in the case of GaN [7]. The N-rich condition provides the best opportunity for Be to substitute for Al. Therefore, the formation energy of Be_{Al} is lower for N-rich condition. Unfortunately, according to our calculations, Be_{Al} is also a rather deep acceptor with the ionization energy of 0.67 eV (almost the same as Mg_{Al}). Under Al-rich condition, Be_{int} has low formation energy and can compensate the Be_{Al} if there is no other lower energy donor. Therefore, it is difficult to dope Be into AlN and avoid compensating Be_{int} under Al-rich conditions. N-rich is a better condition for doping Be mainly because Be_{int} has higher formation energy. However, the fact that Be_{Al} has high ionization energy makes it a poor *p*-type dopant in AlN.

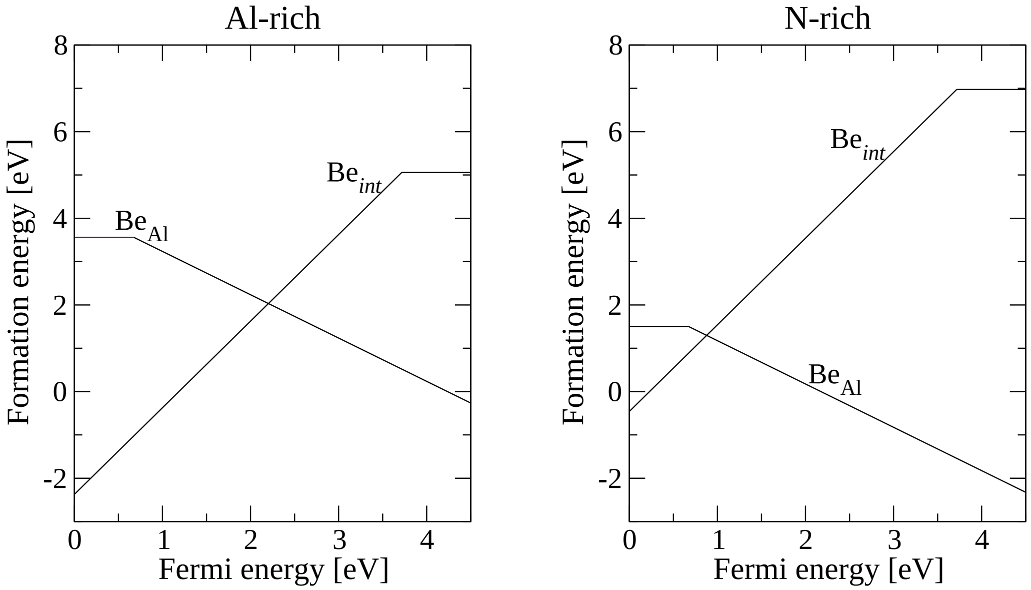

Figure 5: Calculated formation energy as a function of the Fermi level for Be_{Al} and Be_{int} under the Al-rich (left) and N-rich (right) limits. The Fermi level is references to the top of the AlN VBM.

Interstitial gallium and gallium vacancy complexes (Frenkel pairs) in GaN

Native defects can agglomerate into complexes during the growth process, or subsequently cool down after post-annealing.[9-11] Their existences can affect the intentional dopants or the electrical property to the samples.[12] One of the direct approaches to create large amount of native defects is the electron irradiation process. After electron irradiation process, interstitials and the corresponding vacancies are expected. Depending on the energy of the irradiated electron, Ga or N can be selectively knocked out of their sits. There are many experimental works on the electronic and optical properties of samples after electron irradiation in GaN. The attempts to detect these defects have been carried out.[13-17] However, theoretical studies on these complexes are scarce. In this program, we focused our attentions on a complex which consists of an interstitial gallium and gallium vacancy ($\mathrm{Ga}_i - V_{\mathrm{Ga}}$), so-called "gallium-Frenkel pair". These defects are expected to form under high energy electron irradiation. Here, we have performed first principles supercell calculations of gallium-Frenkel complex as well as relevant defects in wurtzite GaN. The possible configurations and the migration mechanism as well as the corresponding energy barriers are investigated. For the migration study, the nudge elastic band (NEB) method [18] was used.

Configurations of gallium Frenkel pairs ($\mathrm{Ga}_i - V_{\mathrm{Ga}}$ *)*

The parent defects of gallium-Frenkel pair are interstitial Ga (Ga_i) and Ga vacancy (V_{Ga}). Gallium interstitial can occur in 3+, 2+, and 1+ charge states, depending on the Fermi energy of the sample. In its 3+ charge state, Ga_i^{3+} favors a site near the octahedral interstitial site. This site locates along the center of hexagonal channel which is called O' site [19]. This O' is only 0.16 Å away from an ideal O site (the symmetric site by symmetry). At O' site the distance to the six Ga nearest neighbors are roughly the same (to within 0.15 Å). The defect level of Ga_i is found to lie in the upper part of the band gap and has *s*-character. The level is completely occupied in 1+ charge state and empty in 3+ charge state. Gallium vacancy can occur in 3–, 2–, 1–, and neutral charge states. The defect levels are raised up from the nitrogen dangling bonds, combined into t_2-states. The t_2-states are split into a doublet and singlet states [20] where the singlet states locate under valence-band maximum (VBM), thus are already occupied and the doublet state lie near above VBM. In the neutral charge state the doublet states have only one electron occupied. They can be filled with up to three more electrons.

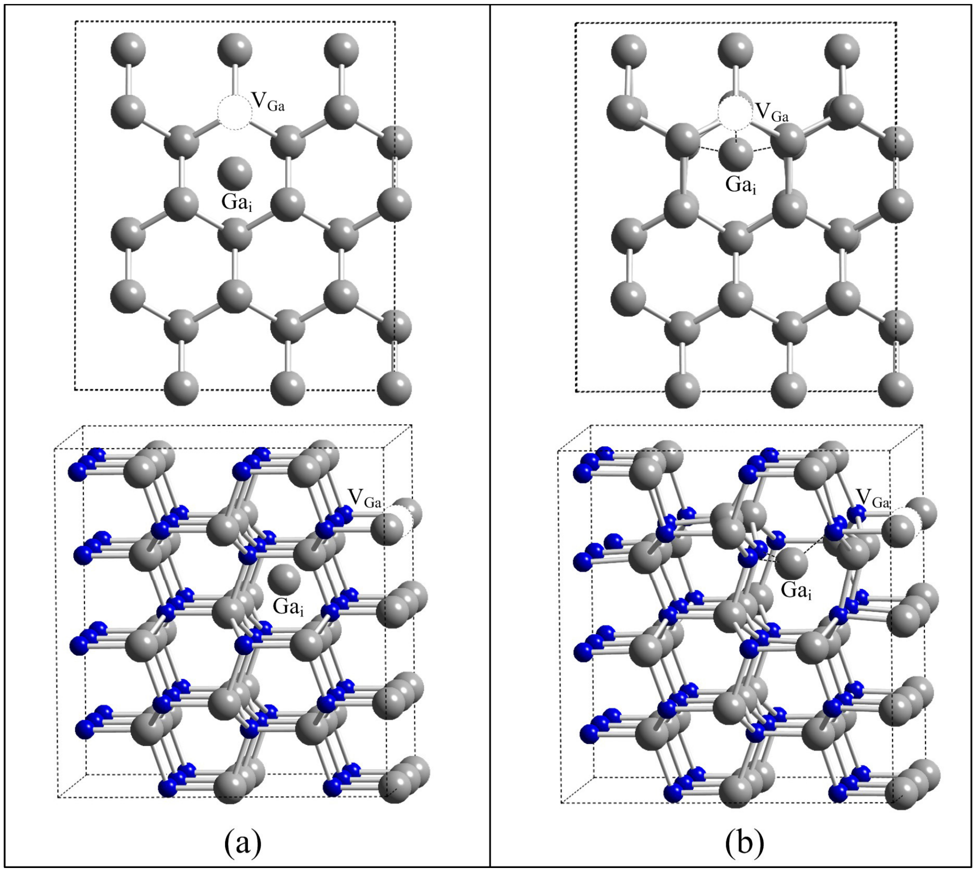

Figure 6: Atomic structure of the lowest energy Ga-Frenkel pair (1st Ga_i-V_{Ga}) from our calculations: (a) before relaxation and (b) after relaxation. Top panels show a top view and lower panels a perspective view.

Because Ga_i and V_{Ga} have opposite charge, they have Coulom attraction to each other. However, if the two defects are placed next to each other, they are spontaneously recombined (Ga_i moves into the center of V_{Ga} and the two annihilated). Even if Ga_i is placed at the next nearest neighbor of V_{Ga}, Ga_i can still spontaneously diffuse *via* the kick-out mechanism and the defects are annihilated. The first stable $\mathrm{Ga}_i - V_{\mathrm{Ga}}$ configuration occurs when the pair is separated by ~ 4 Å along the hexagonal channel in which Ga_i is placed at octahedral site as shown in Fig. 6 (a). Our calculations show that all attempts to place with two defects with the separating distance of less than this would lead to spontaneous annihilation. The configuration in Fig. 6 is labeled

"1^{st} $\mathrm{Ga}_i - V_{\mathrm{Ga}}$", where 1^{st} is denoted for the lowest formation energy. We found that after relaxation the Ga_i has moved by 0.56 Å along the [-1100] direction and subsequently impels the two nearest Ga atoms toward the vacancy with a large displacement of 1.17 Å (see Fig. 6(b)). In the process, a nitrogen atom which has one broken bond, resulting from removal of a Ga atom, relaxed outward significantly.

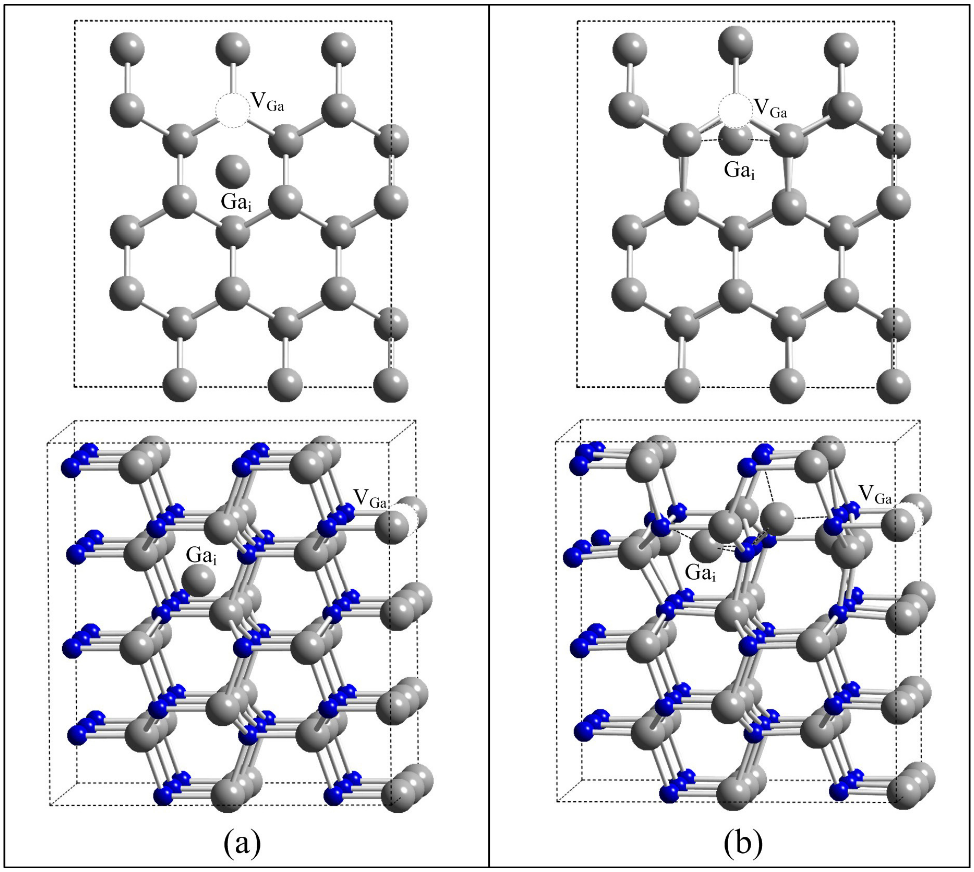

Figure 7: Atomic structure of the Ga-Frenkel pair in 2^{st} Ga_i-V_{Ga} configuration from our calculations: (a) before relaxation and (b) after relaxation. Top panels show a top view and lower panels a perspective view.

The next stable configuration with the higher energy, labeled 2^{nd} $\mathrm{Ga}_i - V_{\mathrm{Ga}}$ is found when the Ga_i is placed at the next nearest octahedral site along the hexagonal channel with a distance of 6.4 Å away from the ideal V_{Ga} position, as shown in Fig 7 (a). After relaxation, the Ga_i spontaneously move toward three nitrogen atoms with a distance of 0.88 Å along [-1100] direction, result in repulsion to the nearby Ga atom which is moved off its site by ~ 1.3 Å toward the closest nitrogen atom with a broken bond.

Beyond the 2^{nd} $\text{Ga}_i - V_{\text{Ga}}$, we have also searching for the next non-recombined configurations. However, we found that the 3^{rd} and 4^{th} non-recombined $\text{Ga}_i - V_{\text{Ga}}$ pairs have almost no binding as will be illustrated next.

Energies of gallium Frenkel complexes.

Figure 8 show the calculated formation energies as a function of Fermi energy in Ga-rich conditions. Note that the total formation energy of $\text{Ga}_i - V_{\text{Ga}}$ pair would be the same for both Ga-rich and N-rich conditions.

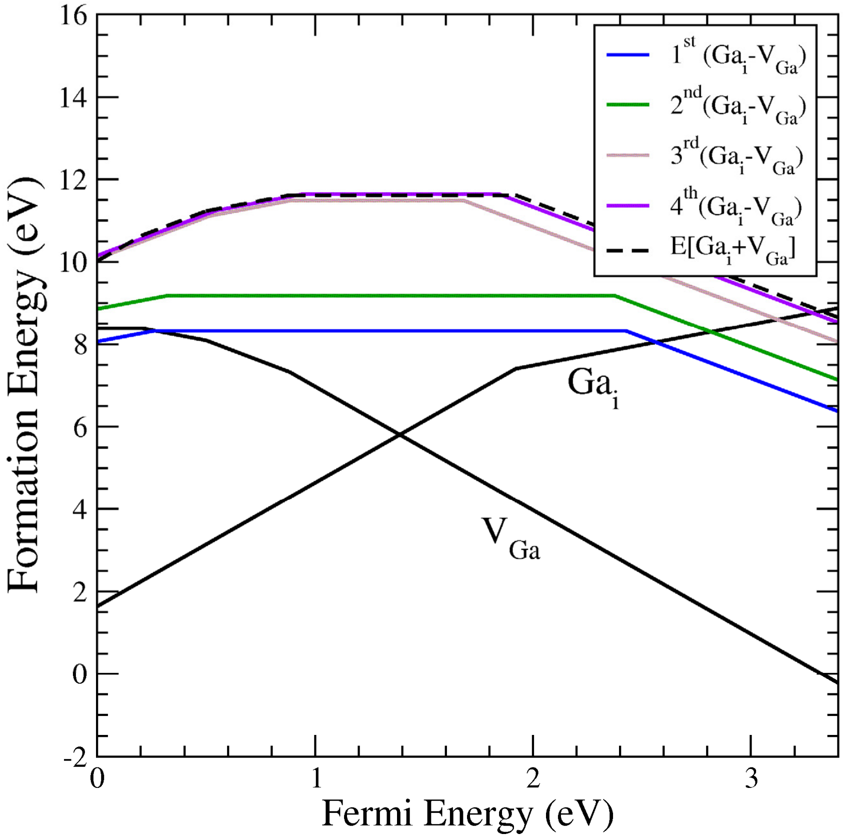

Figure 8: Formation energies as a function of Fermi energy for Ga_i, V_{Ga},and Ga-Frenkel pair (Ga_i-V_{Ga}) under Ga-rich condition. Fermi energy is referenced to the AlN VBM. The labels n^{th} where n =1, 2, 3, 4 are referred to the lowest to highest formation energy of the Frenkel pairs which is also corresponding to the pair separation from smallest to the largest distance.

The calculated defect levels of isolated Ga_i and V_{Ga} are similar to those reported in Ref [19, 20]. Ga interstitial can donate up to 3 electrons. As the Fermi energy is raised the *s*-like defect state near the CBM can be populated by two electrons; turning the defect into 1+ charge state. Note that, the 2+ charge state is never stable (Ga_i is a negative-*U* system). Ga_i acts exclusively as a donor. The defect level of Ga_i is found at approximately 2 eV above the VBM; leading to the transition level $\varepsilon(3+/1+) \approx 2$ eV above the VBM.

In the neutral charge state V_{Ga} is triply occupied, with defect levels lie close to the VBM. These levels are derived from nitrogen *p*-states which have *t*2 symmetry and can accept three more electrons; making V_{Ga} a (deep) triple acceptor. As the Fermi energy is raised, the defect states can be occupied one-by-one resulting in 1–, 2– and 3– charge states [20]. These levels lead to the transition levels $\varepsilon(0/-)$, $\varepsilon(-/2-)$, and $\varepsilon(2-/3-)$ of 0.2 eV, 0.5 eV and 0.9 eV, respectively.

The calculated formation energies for the four considered configurations of $\mathrm{Ga}_i - V_{\mathrm{Ga}}$ pair as a function of Fermi energy are shown in Fig. 8. The formation of $\mathrm{Ga}_i - V_{\mathrm{Ga}}$ follows the reaction: $\mathrm{Ga}_i + V_{\mathrm{Ga}} \rightarrow (\mathrm{Ga}_i - V_{\mathrm{Ga}})$ where the binding energy (E_{bind}) is defined as the difference between the sum of Ga_i and V_{Ga} energies (shown as dashed lines in Fig. 8) and the energy of $\mathrm{Ga}_i - V_{\mathrm{Ga}}$. For neutral $\mathrm{Ga}_i - V_{\mathrm{Ga}}$, the binding energy is defined as $E_{\mathrm{bind}}(\mathrm{Ga}_i - V_{\mathrm{Ga}}) = E^f[(\mathrm{Ga}_i - V_{\mathrm{Ga}})^0] - E^f[\mathrm{Ga}_i^{3+}] - E^f[V_{\mathrm{Ga}}^{3-}]$. We find that only the first two lowest energy configurations (1st and 2nd $\mathrm{Ga}_i - V_{\mathrm{Ga}}$) give reasonably large binding energies ~ 3.3 and 2.4 eV. The other two configurations (with larger separation) have very little binding energy (~ 0.1 eV); implying that they are not stable. The large binding energy of the 1st and 2nd $\mathrm{Ga}_i - V_{\mathrm{Ga}}$ configurations indicates that they are stable against the decomposition into isolate parent defects. (However, whether they are stable against annihilation into a perfect crystal is subject to further investigations.) The large binding energies of 1st and 2nd $\mathrm{Ga}_i - V_{\mathrm{Ga}}$ configurations can be explained by Coulomb attraction between the opposite charges of Ga_i^{3+} and V_{Ga}^{3-}.

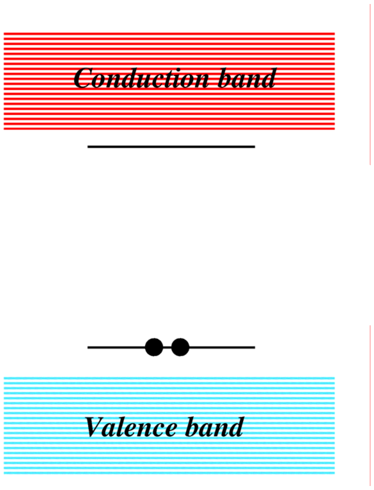

Figure 9: Schematic illustration of the defect levels induced by the 1st Ga_i-V_{Ga} configuration in the GaN band gap. The solid dots show the electron occupation for the neutral charge state.

The schematic illustration for electronic level in neutral charge state induced by the 1st $\mathrm{Ga}_i - V_{\mathrm{Ga}}$ configuration is shown in Fig 9. This indicates that the defect complex is electrically inactive at almost entire Fermi energy range except near the band edges. The 2nd $\mathrm{Ga}_i - V_{\mathrm{Ga}}$ configuration exhibits similar electronic levels with slight variation in the positions (not shown).

Formations and separations of gallium Frenkel complex.

To investigate the energy of $\mathrm{Ga}_i - V_{\mathrm{Ga}}$ as a function of the pair separation, we calculated the energy profile of the pair separation by using nudge elastic band method (NEB). The calculation is started with a defect-free GaN bulk supercell as a ground-state configuration. Then, a Ga atom is dislocated out from its site to the nearest interstitial site; leaving a vacancy behind. Next, the Ga_i atom is migrate further to form the 1st $\mathrm{Ga}_i - V_{\mathrm{Ga}}$ configuration by the kick-out mechanism [19]. The energy profile for the migration is mapped by using the NEB method [18]. As the next step, the energy profile in the further migration from the 1st $\mathrm{Ga}_i - V_{\mathrm{Ga}}$ configuration to the 2nd Ga_i-V_{Ga} configuration is mapped out. It is found that the energy needed for migration from ground state to the 1st Ga_i-V_{Ga} configuration is ~ 8.33 eV which is the formation energy of 1st Ga_i-V_{Ga} configuration. Additional energy of 0.86 eV is needed to further transform into the 2nd Ga_i-V_{Ga} configuration. Overall, this entire profile shows that the 1st (as well as 2nd) Ga_i-V_{Ga} configuration is metastable and, in principle, can be stabilized. However, they can be recombined if the Ga_i atom gains sufficient energy to overcome the barriers which are 0.17 eV and 0.04 eV for the 1st and 2nd Ga_i-V_{Ga} configuration, respectively. Since Ga_i is known to be very diffusive at room temperature [3, 16], the Ga_i-V_{Ga} is unlikely to be stable unless the sample is kept at low temperature. This energy profile could be used for further study of Ga_i-V_{Ga} complex formations by other approaches such as Monte Carlo method.

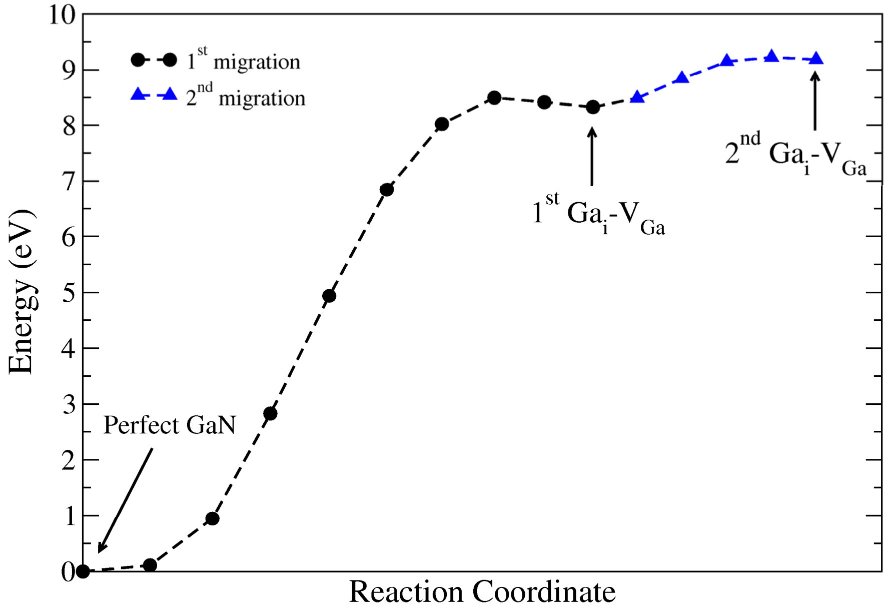

Figure 9: Calculated energy profile of the gallium Frenkel defects. Starting from the perfect GaN bulk to the 1st (solid dots) and 2nd Ga_i-V_{Ga} (solid triangles) configurations.

CN and SiN complexes in dilute nitrides (GaAs:N and GaP:N)

In dilute nitrides, the nitrogen atoms are not fitted well into the anion site due to its small size. As a result, the nitrogen is highly strained. On the other hand, the diatomic molecule such as N_2, NO, O_2, CN or SiN is slightly bigger and can substitute on the anion size with a reasonable energy. As a result, when there are impurities or intentionally doped elements, such as C or Si, the diatomic substitution on the anion site such as CN_{As} and SiN_{As} can form.

CN complexes in diluted nitrides

CN molecules in GaAs and GaP have been studied. Two possible lattice locations: (1) CN molecules substituting for anions (CN_{As} or CN_P), as shown in Fig. 10 and (2) interstitial CN molecules at the T_d site surrounded by four Ga atoms (CN_i) are investigated. All possible charge states and various orientations were considered. Calculated formation energies show that the molecule favors substituting for the anion site over the interstitial configuration for all equilibrium growth conditions with a margin of at least 1 eV. The calculations predict the CN molecule to produce a level with a strong $pp\pi^*$ molecular orbital characteristic at approximately 0.5 - 0.8 eV above the VBM. In *p*-type conditions, where the Fermi level is located below this $pp\pi^*$ level, the molecules are triply bonded and form donor defect centers (double donor CN_{As}^{2+} and single donor CN_i^{1+}). The calculations with full relaxation show that triply bonded CN_{As}^{2+} and CN_i^{1+} do not orient symmetrically in the Ga tetrahedron but instead are tilted in order to gain better interactions with neighboring Ga atoms. The calculated vibration frequencies of the triply boned CN_{As}^{2+} and CN_i^{1+} are in reasonable agreement with the measurement by Ulrici and Clerjaud [21] supporting their identification that the bonding is triple-bond type. Although neither CN_{As} nor CN_i have the C-N bond oriented along the <100> directions as proposed by Ulrici and Clerjaud, the low rotation barrier of CN_{As}^{2+} makes it possible that the molecule might be constantly rotating, leading to an average orientation in the <100> direction. At higher Fermi level, the CN_i^{1+} can accept an electron and becomes CN_i^0 whereas CN_{As}^{2+} can accept 1, 2, 3, or 4 electrons (depending on the Fermi level) and becomes CN_{As}^{1+}, CN_{As}^{0} (metastable), CN_{As}^{1-}, or CN_{As}^{2-}, respectively. We found that the C-N bond length and vibrational frequency change linearly (to a good approximation) with the number of electrons added into the antibonding states of the molecule.

Further details of this work can be found in an attached manuscript [P2].

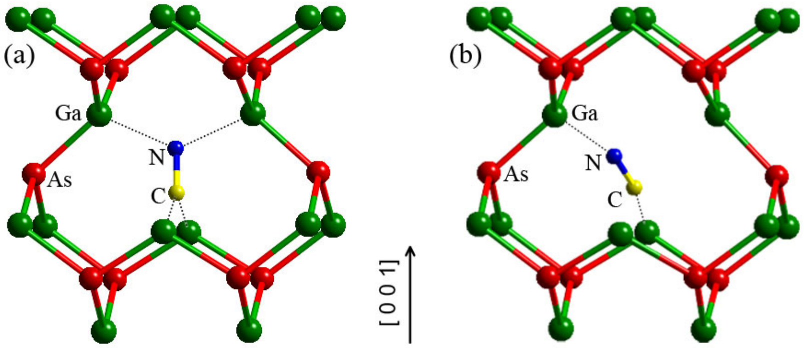

Figure 10: Local atomic geometry of a CN molecule substituting on an As site in GaAs: (a) symmetric configuration, CN_{As}(sym) and (b) asymmetric configuration, CN_{As}(asym). Both are shown for charge state 2+.

SiN complexes in diluted nitrides

Yu *et al.* [22] reported that when $GaAs_{1-x}N_x$ is doped with Si, the interaction between Si and N leads to a ‘‘mutual passivation,’’ characterized by an increase in the band gap and an elimination of the electrical activity of the Si donor. We found that the SiN molecule substituting on the As site (SiN_{As}) provide a better model to explain the mutual passivation of shallow donor Si and isovalent N in dilute GaAsN alloys. Instead of the recently proposed pairing of Si and N on adjacent substitutional sites (Si_{Ga}-N_{As}) [22, 23] we find that N changes the behavior of Si in dilute nitride alloys in a more dramatic way. N and Si combine into a deep-acceptor split interstitial, where Si and N share an As site SiN_{As}, with a significantly lower formation energy than that of the Si_{Ga}-N_{As} pair in *n*-type GaAs and dilute GaAsN alloys. The formation of SiN_{As} explains the GaAs band-gap recovery and the appearance of a photoluminescence peak at 0.8 eV. This model can also be extended to Ge-doped GaAsN alloys, and correctly predicts the absence of mutual passivation in the case of column-VI dopants. This work has been published in Phys. Rev. Lett. [12]

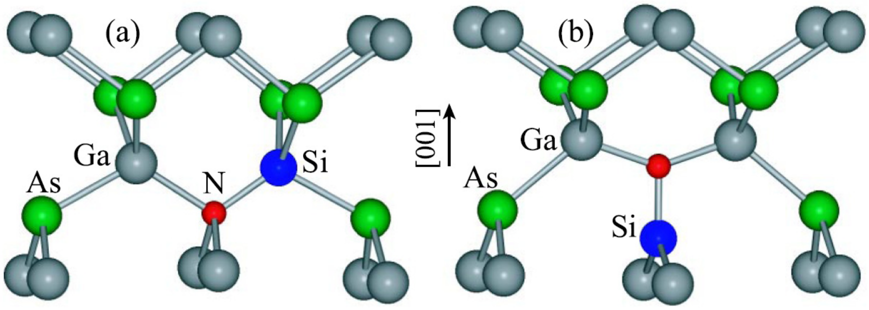

Figure 11: Local structure of (a) $(Si_{Ga}\text{-}N_{As})^+$ and (b) $(SiN_{As})^-$. In the Si_{Ga}-N_{As} configuration, Si_{Ga} is a nearest neighbor of N_{As}; in the SiN_{As} configuration, Si and N share an As site.

Local structure of Indium oxynitride (InON) from x-ray absorption spectroscopy

Indium oxynitride can be considered as an alloy between indium nitride (InN) and indium oxide (In_2O_3). The two parent compounds have very different crystal structures. In this work, the local structures of indium oxynitride (InO_xN_{1-x}) with varied O contents, prepared by rf magnetron sputtering, were identified by using a combination of first-principles calculations and synchrotron x-ray absorption near edge structures (XANES). The InO_xN_{1-x} samples were characterized by indium *L*3-edge XANES measurements at Synchrotron Light Research Institute in Thailand. To understand the local structures of the samples, we independently performed first-principles indium *L*3-edge simulations of wurtzite InN, wurtzite $InN_{0.6}O_{0.4}$, and bixbyite In_2O_3 crystals. The measured XANES spectrum of sample, with no intentionally doped O, is in agreement with the simulated spectrum of pure wurtzite InN. The spectrum of the sample, which contains only O, is also in agreement with the simulated spectrum of pure bixbyite In_2O_3. Interestingly, the spectrum of sample containing ~40% of O ($InN_{0.6}O_{0.4}$) is almost identical to that of pure InN except at low energy range. This provides strong evidence that the structure of the sample remains wurzite like that of pure InN. For the sample containing more than 40% of O, the spectra show a mixed signature between that of wurtzite ($InN_{0.6}O_{0.4}$) and bixbyite (In_2O_3) structures. This work illustrates that XANES is a powerful technique for identification of local structures, especially when it is used in conjunction with first principles calculations.

Further details of this work can be found in an attached manuscript [P1].

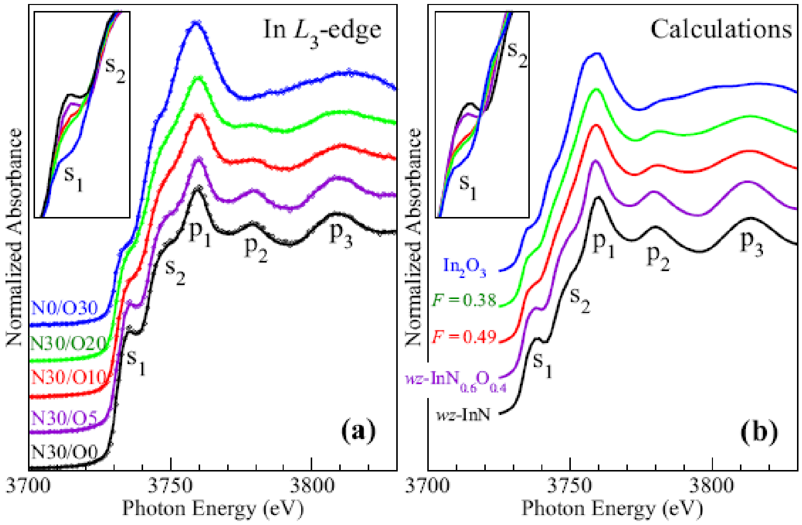

Figure 12: (a) The measure XANES spectrum of InO_xN_{1-x} samples at different N/O ratio. (b) An independently simulated spectra. The insets show the zoom-up of the pre-edge regions.

Hydrogen site in ZnO: the role of Ca impurity

In 2000, Van de Walle, proposed that H prefers to form a strong O-H bond with lattice O and acts exclusively as a donor, H^+ [24]. This behavior is different from H in almost all other semiconductors in which H is amphoteric, counteracting the dominant dopant [25]. The prediction that H is an exclusive donor stirred up considerable research activities, because it may explain the difficulty in the *p*-doping [26-34]. Although, it is clear that H^+ prefers to bind strongly with O at a bond length of approximately 1 Å and with a vibration frequency around 3500 cm^{-1}, the details is completely controversial: McCluskey *et al.* [29] observed an IR peak at 3326 cm^{-1} in samples provided by Cermet, while Lavrov *et al.* [35] observed a different peak at 3611 cm^{-1} in samples by Eagle-Picher. This indicates that there exist two forms of O-H in these two types of samples. These 3326 and 3611-cm^{-1} IR peaks are consistent with the calculated frequencies of H at the antibonding and bond-center sites, respectively. Based on first principles calculations, we showed that Ca, found only in Cermet samples, plays a pivotal role in switching the H from the bond-center site to the anti-bonding site. We found that with Ca, the anti-bonding site is 0.5 eV more stable than the ground-state bond-center site in pure, Ca-free ZnO.

Further details of this work can be found in an attached manuscripts [P3][P4].

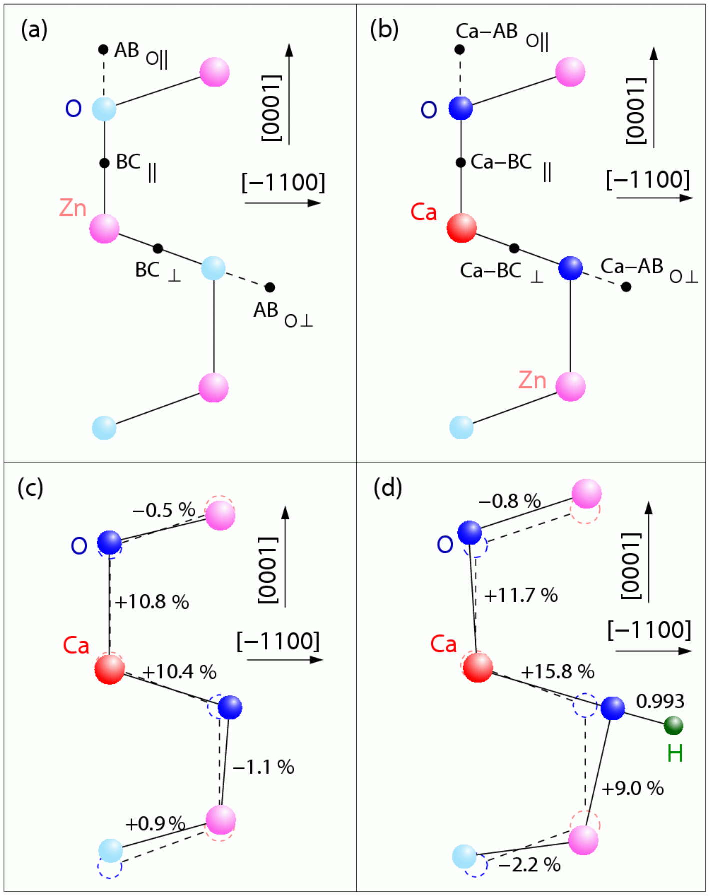

Figure 13: Schematic drawings the four H$^+$ sites in Ca-free ZnO and near a Ca impurity. Calculated atomic relaxations of Ca-AB$_{O\perp}$ (c) in the absence and (d) in the presence of H$^+$.

Examples of Future Research Activities

Binding between Mg_{Al} *and* Mg_{int} *(as well as between* Be_{Al} *and* Be_{int}*) in* AlN

In order for Mg and Be to be a good *p*-type dopant in AlN, it is also important that the self compensations can be controlled. In GaN, our calculations have shown that Be could be a superior *p*-type dopant over Mg when Be is substituting for Ga. However, due to a smaller size of Be, the interstitial form of Be in GaN also have rather low formation energy, especially when the sample is *p*-type. The similar study will be repeated for AlN.

Roles of native defects in III-N alloys

In this program the native defects in AlN has been studied. This new result, combining with the earlier studied of native defects in GaN, gives us a more complete picture of the native defects in this class of compounds. However, most III-nitride devices use the alloys not just the parent compounds. Therefore, native defects in alloys should be directly studied. We will directly study the properties of native defects in alloys in the next program.

Statistical analysis of Frenkel pair stability

Based on the calculated energy of (Ga) Frenkel pair *vs* separation of the pair obtained from this program, the stability of the Frenkel pair can be further modeled by using Monte Carlo method. From the energy profile, the realistic simulation of the creation of the Frenkel pair by electron irradiation under different flux, electron energy, and temperature of the system can be made.

Nitrogen Frenkel pair in GaN

To complete the Frenkel pair study, the nitrogen Frenkel pair will be investigated. Nitrogen Frenkel pair composed of a nitrogen interstitial and a nitrogen vacancy forming a pair. The properties and the stability of nitrogen Frenkel pair could be very different from Ga Frenkel. This is because the nitrogen interstitial is actually in the split interstitial form (two N atoms forming an N_2 and sharing a nitrogen site).

References

[1] http://cms.mpi.univie.ac.at/vasp/.

[2] http://leonardo.phys.washington.edu/feff/.

[3] S. Limpijumnong and C. G. Van de Walle, Phys. Rev. B **69**, 035207 (2004).

[4] S. Na-Phattalung, M. F. Smith, K. Kim, M.-H. Du, S.-H. Wei, S. B. Zhang, and S. Limpijumnong, Phys. Rev. B **73**, 125205 (2006).

[5] C. Stampfl and C. G. Van de Walle, Phys. Rev. B **65**, 155212 (2002).

[6] S. Limpijumnong, X. Li, S.-H. Wei, and S. B. Zhang, Appl. Phys. Lett. **86**, 211910 (2005).

[7] C. G. Van de Walle, S. Limpijumnong, and J. Neugebauer, Phys. Rev. B **63**, 245205 (2001).

[8] Y. Taniyasu, M. Kasu, and T. Makimoto, Nature **441**, 325 (2006).

[9] J. Neugebauer and C. G. Van de Walle, Phys. Rev. Lett. **75**, 4452 (1995).

[10] D. J. Chadi, Appl. Phys. Lett. **71**, 2970 (1997).

[11] T. Mattila and R. M. Nieminen, Phys. Rev. B **55**, 9571 (1997).

[12] A. Janotti, P. Reunchan, S. Limpijumnong, and C. G. Van de Walle, Phys. Rev. Lett. **100**, 045505 (2008).

[13] D. C. Look, D. C. Reynolds, J. W. Hemsky, J. R. Sizelove, R. L. Jones, and R. J. Molnar, Phys. Rev. Lett. **79**, 2273 (1997).

[14] D. C. Look, Materials Science and Engineering B **80**, 383 (2001).

[15] Z. Q. Fang, J. W. Hemsky, D. C. Look, and M. P. Mack, Appl. Phys. Lett. **72**, 448 (1998).

[16] K. H. Chow, G. D. Watkins, A. Usui, and M. Mizuta, Phys. Rev. Lett. **85**, 2761 (2000).

[17] L. S. Vlasenko, C. Bozdog, G. D. Watkins, F. Shahedipour, and B. W. Wessels, Phys. Rev. B **65**, 205202 (2002).

[18] H. Jónsson, G. Mills, and K. W. Jacobsen, in *Classical and Quantum Dynamics in Condensed Phase Simulations*, edited by B. J. Berne, G. Ciccotti, and D. F. Coker (World Scientific, Singapore, 1998), p. 385.

[19] S. Limpijumnong and C. G. Van de Walle, Phys. Rev. B **69**, 035207 (2004).

[20] J. Neugebauer and C. G. Van de Walle, Phys. Rev. B **50**, 8067 (1994).

[21] W. Ulrici and B. Clerjaud, Phys. Rev. B **72**, 045203 (2005).

[22] K. M. Yu, W. Walukiewicz, J. Wu, D. E. Mars, D. R. Chamberlin, M. A. Scarpulla, O. D. Dubon, and J. F. Geisz, Nat Mater **1**, 185 (2002).

[23] J. Li, P. Carrier, S.-H. Wei, S.-S. Li, and J.-B. Xia, Phys. Rev. Lett. **96**, 035505 (2006).

[24] C. G. Van de Walle, Phys. Rev. Lett. **85**, 1012 (2000).

[25] C. G. Van de Walle and J. Neugebauer, Nature **423**, 626 (2003).

[26] K. Ip, M. E. Overberg, Y. W. Heo, D. P. Norton, S. J. Pearton, C. E. Stutz, B. Luo, F. Ren, D. C. Look, and J. M. Zavada, Appl. Phys. Lett. **82**, 385 (2003).

[27] S. J. Jokela and M. D. McCluskey, Phys. Rev. B **72**, 113201 (2005).

[28] E. V. Lavrov and J. Weber, Phys. Rev. B **73**, 035208 (2006).

[29] M. D. McCluskey, S. J. Jokela, K. K. Zhuravlev, P. J. Simpson, and K. G. Lynn, Appl. Phys. Lett. **81**, 3807 (2002).

[30] G. A. Shi, M. Stavola, S. J. Pearton, M. Thieme, E. V. Lavrov, and J. Weber, Phys. Rev. B **72**, 195211 (2005).

[31] K. Shimomura, K. Nishiyama, and R. Kadono, Phys. Rev. Lett. **89**, 255505 (2002).

[32] S. F. J. Cox, E. A. Davis, S. P. Cottrell, P. J. C. King, J. S. Lord, J. M. Gil, H. V. Alberto, R. C. Vilão, J. Piroto Duarte, N. Ayres de Campos, A. Weidinger, R. L. Lichti, and S. J. C. Irvine, Phys. Rev. Lett. **86**, 2601 (2001).

[33] C. H. Seager and S. M. Myers, J. Appl. Phys. **94**, 2888 (2003).

[34] M. D. McCluskey and S. J. Jokela, Proceedings of the NATO Advanced Workshop on Zinc Oxide, edited by N. Nickel and E. Terukov, NATO Science Series II **194**, 125 (2005).

[35] E. V. Lavrov, J. Weber, F. Börrnert, C. G. Van de Walle, and R. Helbig, Phys. Rev. B **66**, 165205 (2002).

Related Activities:

Publications (attached)

[P1] "*Local structure of indium oxynitride from x-ray absorption spectroscopy*"
J. T-Thienprasert, J. Nukeaw, A. Sungthong, S. Porntheeraphat, S. Singkarat,
D. Onkaw, S. Rujirawat, and S. Limpijumnong
Appl. Phys. Lett. **93**, 051903 (2008).

[P2] "*Carbon-nitrogen molecules in GaAs and GaP*"
Sukit Limpijumnong, P. Reunchan, A. Janotti, and C.G. Van de Walle
Phys. Rev. B **77**, 195209 (2008).

[P3] "*Hydrogen in ZnO revisited: Bond center versus antibonding site*"
X.-B. Li, Sukit Limpijumnong*, W.Q. Tian, H.-B. Sun, and S.B. Zhang
Phys. Rev. B **78**, 113203 (2008).

[P4] "*An unexpected Coulomb binding between* Ca *and* H^+ *in* ZnO"
X.-B. Li, Sukit Limpijumnong, W.Q. Tian, and S.B. Zhang
J. Vac. Sci. Technol. B **27**, 1601 (2009).

Presentations

[C1] Sukit Limpijumnong delivered an invited talk at the 5th Thai Summer School of Computational Chemistry at Suranaree Univ. of Tech., Thailand, October 14, 2008, entitled: *"Structure of hydrated ions: A combined Synchrotron XAS experiments and quantum mechanical simulations study"*.

[C2] Sukit Limpijumnong delivered an invited talk at the 13th Annual Symposium on Computational Science and Engineering at Kasetsart University, Thailand, March 26, 2009, entitled: *"Crystal phase transformations under specific loading conditions"*.

[C3] Sukit Limpijumnong delivered a seminar at Seoul National University, South Korea, April 2, 2009, entitled: *"Verification of defect structures by x-ray absorption spectroscopy"*.

Collaborations

1. Dr. David C. Look (experiment), *Wright-Patterson Air Force Base, OH, USA*
2. Dr. S.B. Zhang (theory), *Rensselaer Polytechnic Institute, NY, USA*
3. Drs. S-H. Wei and K. Kim (theory), *National Renewable Energy Lab., CO, USA*.
4. Drs. X. Li and T.J. Coutts (experiment), *National Renewable Energy Lab., CO, USA*.
5. Prof. Dr. Weimin Chen (experiment), *Linköpin University, Sweden*.
6. Prof. Dr. W.R.L. Lambrecht (theory), *Case Western Reserve Univ., OH, USA*.
7. Prof. Dr. C.G. Van de Walle (theory), *UC Santa Barbara, CA, USA*.
8. Prof. Dr. Jiti Nukeaw (experiment), *King Mongut's Institute of Tech., Thailand*

Honors/Awards

- Prof. Sukit Limpijumnong has been named " *2008 TRF Advanced Research Scholar* " by the Thailand Research Fund (TRF)
- Prof. Sukit Limpijumnong has been appointed as " *APCTP General Council Member 2008-2010"* by the Asia Pacific Center for Theoretical Physics (APCTP), South Korea
- Prof. Sukit Limpijumnong has been appointed as *"TWAS Young Affiliate 2007-2012"* by the Third World Academy of Science (TWAS), Italy

Appendix

Publications

1. "*Local structure of indium oxynitride from x-ray absorption spectroscopy*"
   J. T-Thienprasert, J. Nukeaw, A. Sungthong, S. Porntheeraphat, S. Singkarat, D. Onkaw, S. Rujirawat, and S. Limpijumnong
   Appl. Phys. Lett. **93**, 051903 (2008).
2. "*Carbon-nitrogen molecules in GaAs and GaP*"
   Sukit Limpijumnong, P. Reunchan, A. Janotti, and C.G. Van de Walle
   Phys. Rev. B **77**, 195209 (2008).
3. "*Hydrogen in ZnO revisited: Bond center versus antibonding site*"
   X.-B. Li, Sukit Limpijumnong*, W.Q. Tian, H.-B. Sun, and S.B. Zhang
   Phys. Rev. B **78**, 113203 (2008).
4. "*An unexpected Coulomb binding between* Ca *and* H^+ *in* ZnO"
   X.-B. Li, Sukit Limpijumnong, W.Q. Tian, and S.B. Zhang
   J. Vac. Sci. Technol. B **27**, 1601 (2009).

APPLIED PHYSICS LETTERS **93**, 051903 (2008)

Local structure of indium oxynitride from x-ray absorption spectroscopy

J. T-Thienprasert,[1] J. Nukeaw,[2] A. Sungthong,[2] S. Porntheeraphat,[3] S. Singkarat,[4]
D. Onkaw,[1] S. Rujirawat,[1] and S. Limpijumnong[1,a)]
[1]*School of Physics, Suranaree University of Technology and National Synchrotron Research Center, Nakhon Ratchasima 30000, Thailand*
[2]*Nanotechnology Research Center of KMITL and Department of Applied Physics, King Mongkut's Institute of Technology Ladkrabang, Bangkok 10520, Thailand*
[3]*Thai Microelectronics Center, National Electronics and Computer Technology Center, Pathumthani 12120, Thailand*
[4]*Fast Neutron Research Facility, Faculty of Science, Chiang Mai University, Chiang Mai 50200, Thailand*

(Received 23 May 2008; accepted 10 July 2008; published online 5 August 2008)

Synchrotron x-ray absorption near edge structures (XANES) measurements of In L_3 edge is used in conjunction with first principles calculations to characterize rf magnetron sputtered indium oxynitride at different O contents. Good agreement between the measured and the independently calculated spectra are obtained. Calculations show that the XANES spectra of this alloy are sensitive to the coordination numbers of the In atoms, i.e., fourfold for indium nitride-like structures and sixfold for indium oxide-like structures, but not to the substitution of nearest neighbor N by O or vice versa. © *2008 American Institute of Physics*. [DOI: 10.1063/1.2965802]

Indium oxynitride can be considered as an alloy between indium nitride (InN) and indium oxide (In_2O_3). This is unlike most of the traditional semiconductor alloys in the sense that the crystal structures as well as the anion valencies of the two parent compounds are different. InN is one of the highly studied III-nitride semiconductors (GaN, AlN, and InN) because III-nitride alloys are widely used for optoelectronic applications. Despite real applications and substantial research in III-nitride materials, InN bandgap has been mistaken to be ~1.9 eV for a long time (see the discussion in Refs. 1 and 2). Only recently, the actual InN bandgap of ~0.7 eV has been realized.[3,4] The apparently large bandgap observed in the past is most likely due to the Moss–Burstein shift caused by substantial unintentional carriers that are typical for InN grown by traditional techniques (dc discharge or sputtering).[1,5–7] Because InN has a (now–realized) small bandgap of ~0.7 eV and In_2O_3 has a large optical gap of ~3.6 eV,[8] the band gap of indium oxynitride can potentially be engineered in a very wide range. This, combining with the availability of low temperature growth techniques, such as rf magnetron sputtering,[9] make indium oxynitride a strong candidate for optical coating applications.

For alloys with low O content, it has been reported that O atoms substitute for N in the wurtzite InN crystal structure.[10] However, in higher O content alloys the crystal structure remains unclear. Previously, an attempt to study indium oxynitride structures by N *K*-edge x-ray absorption near edge structures (XANES) has been done.[11] However, probing local structure of anions in this alloy system is not the most direct way because anions in both InN and In_2O_3 are fourfold coordinated. Unlike anion, the coordination number of In in the two compounds are different, i.e., it is sixfold in In_2O_3 [Fig. 1(a)] and fourfold in InN [Fig. 1(b)]. Therefore, probing the local structure of In atoms should give more direct information on the alloy structures. In this letter, the In L_3-edge XANES is used to characterize indium oxynitride with varied compositions. The XANES has been proven to be a powerful tool in resolving the local structures around the absorbing atoms (in this case In atoms).[12–14]

Indium oxynitride films were grown by rf magnetron sputtering (Edwards Auto 306) at room temperature using a technique called reactive gas timing.[15,16] The growth process started with the preevacuation of the chamber to the order of 10^{-5} Pa. Then N_2 and O_2 gas were flown interchangeably at the flow rate of 10 standard cubic centimeter per minute onto the 99.999% purity In target. The sputtering gas pressures were set at 0.34 and 0.32 Pa for N_2 and O_2, respectively. By controlling N_2 and O_2 gas timing, indium oxynitride samples with varied O contents were obtained. The interval of gas timing cycles used for each sample is shown in Table I and the samples are named according to the gas timing cycles. The rf plasma power was set at 100 W. All samples were grown on polyethylene terephthalate substrate to the thickness of ~1 μm (typical growth time is approximately 1 h). To measure the actual O content in each sample, the [O]:[In] ratios were determined using Auger electron spectroscopy (AES) with capability of sputter depth profiling. The O contents were found to be homogeneous throughout the film thickness. Note that AES measured O in all forms. The optical bandgaps measured by UV-visible spectroscopy were found to increase with O_2 gas timing ratio, as shown in Table I. This is consistent with the work of Yi *et al.*[11] that reported the increase in optical bandgap of indium oxynitride with O content. Although the optical bandgap of N30/O0 sample is

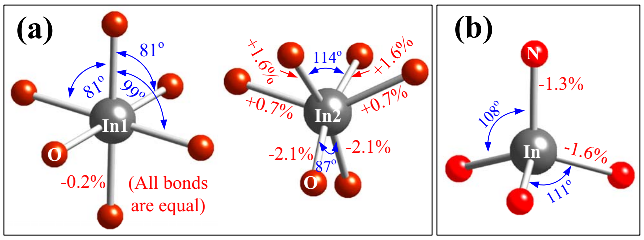

FIG. 1. (Color online) The local structure around In atoms used in the simulations of the In L_3-edge XANES of (a) In_2O_3 and (b) InN. All bond distances are given as a percentage difference from an average In_2O_3 bond distance (d_{calc}=2.170 Å).

[a)] Author to whom correspondence should be addressed. Electronic mail: sukit@sut.ac.th.

TABLE I. The gas timing conditions, optical bandgaps, and [O]:[In] compositions of the samples.

Sample	Gas timing (s)		Optical bandgap (eV)	[O]:[In] composition
	N_2	O_2		
N30/O0	30	0	1.5	0.16
N30/O5	30	5	1.6	0.43
N30/O10	30	10	1.6	0.96
N30/O20	30	20	2.4	1.08
N0/O30	0	30	3.4	1.50

larger than that of pure InN and the sample is expected to contain a few percent of unintentionally doped O, this gap widening in low O samples is most likely due to Moss–Burstein effects[1,5–7] not the changes in the crystal structure. As will be discussed, L_3-edge XANES of In is sensitive to the change in In coordination number but not to the interchanging between N and O. Therefore, XANES of InN with a few percent of N replaced by O are expected to be almost identical to pure InN because they are structurally the same.

The samples were characterized by In L_3-edge XANES measurements in the fluorescent mode with a 13-component Ge detector (Canbera) at the x-ray absorption spectroscopy beamline (BL-8) of the Siam Photon Source (electron energy of 1.2 GeV, beam current 120–80 mA), National Synchrotron Research Center, Thailand. Double crystal monochromator Si (111) was used to scan the synchrotron x ray with the photon energy step of 0.25 eV in the range of 3700 to 3850 eV, covering the XANES region of In L_3 edge. The measured spectra are shown in Fig. 2(a).

In order to understand the local microscopic structure, we performed first principles In L_3-edge XANES simulations of wurtzite InN and bixbyite In_2O_3 crystals. The detailed crystal structures were optimized based on first principles pseudopotential calculations. We used density functional theory with local density approximation and ultrasoft pseudopotentials as implemented in the VASP code.[17] The cutoff energy for the plane wave basis set was set at 400 eV. We used Monkhorst–Pack k-point mesh for Brillouin zone integration ($7\times7\times7$ for InN and $3\times3\times3$ for In_2O_3). All atoms were allowed to relax until the residue forces were less than 10^{-3} eV/Å. The fully relaxed local structures surrounding In atoms are shown in Figs. 1(a) and 1(b) for In_2O_3 and InN, respectively. All In atoms in wurtzite InN crystal are equivalent. However, there are two species of In atoms in In_2O_3, labeled In1 and In2, with the composition ratio of 1:3. These structural relaxations by first principles calculations is a crucial step to obtain the computationally unstrained structures to be further used in XANES calculations.

To calculate *ab initio* XANES of InN and In_2O_3 based on the relaxed crystal structures above, we used FEFF8.2 codes.[18,19] The codes utilize a full multiple scattering approach based on *ab initio* overlapping muffin-tin potentials. The muffin-tin potentials were obtained using self-consistent calculations with Hedin–Lundqvist exchange-correlation function. The self-consistent calculations were performed in the sphere radius 4 Å (~40 atoms) around the absorber In atom, which is more than sufficient to allow charge to fluctuate yielding realistic electron relaxations. The full multiple scattering calculations include all possible paths within a larger cluster radius of 7.4 Å (~140 atoms).

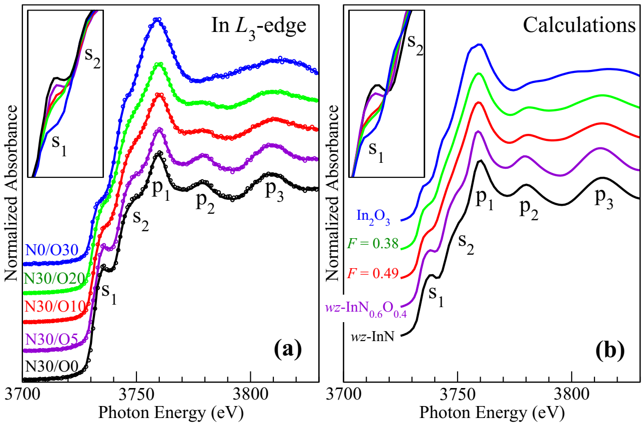

FIG. 2. (Color online) (a) Normalized In L_3-edge XANES spectra of indium oxynitride samples prepared under different gas timing with increased O_2 timing from bottom curve to top curve. Circles show recorded data points and the curves are the (noise removed) fit to the data. Inset: the plots from the main panel without offset at the energy range near the s_1 shoulders to highlight the changes in the shoulder height. (b) The calculated In L_3-edge XANES spectra of wurtzite InN, bixbyite In_2O_3, wurtzite $InN_{0.6}O_{0.4}$, and the simulated separated phase alloys with 38% and 49% fourfold In atoms (see text for detail).

The calculated In L_3-edge spectra of InN and In_2O_3 crystals are shown in Fig. 2(b) (bottom and top curves, respectively). For In_2O_3, because there are two species of nonequivalent In atoms, the spectrum shown is the weight averaged between the spectra from the two species. Note that the spectra obtained from the two species of In in In_2O_3 are very similar. The spectra of fourfold In in InN and sixfold In in In_2O_3 are, however, clearly different; making In L_3-edge XANES a suitable tool to study the local structure around In atoms. Our test calculations also show that the XANES spectra of the fourfold (sixfold) In atom is not very sensitive to the substitution of a neighboring N by O (O by N).[20]

The calculated spectra of InN and In_2O_3 are in full agreement with the measured spectra from N30/O0 and N0/O30 samples, respectively. The main features of InN XANES spectrum is composed of two shoulders and three peaks labeled as s_1, s_2, p_1, p_2, and p_3. All five features are in a very good agreement with the corresponding features in the N30/O0 sample in both positions and shapes. Similar agreement can be found between the spectrum of N0/O30 sample and the calculated In_2O_3 spectrum. This suggests that structurally In atoms in N30/O0 are mostly fourfold (as those in InN) and in N0/O30 are mostly sixfold (as those in In_2O_3). If we compare the measured spectra of different O contents [from the bottom curve to the top curve of Fig. 2(a)], we can see that the five features are progressively evolved as O content increased. The progressive changes include: (1) the reduction in s_1 peak (for clarity, the same set of spectra without offset is shown in the inset), (2) the broadening and increase in magnitude of p_1 peak, (3) the reduction in p_2 peak, and (4) the significant broadening accompanied by a slight shift to higher energy of peak p_3. Interestingly, the spectrum of N30/O5 (at 43% O content) is still almost perfectly overlapped with that of N30/O0 with the exception of s_1 shoulder, which is slightly reduced [see inset of Fig. 2(a)]. This indicates that most of In atoms in N30/O5 remain fourfold and O atoms are substituting on the N sites. To test this assumption, we calculated the XANES spectra for $InN_{0.6}O_{0.4}$ alloy in the wurtzite structure [the second curve from bottom in Fig. 2(b)]. The calculated curve is almost overlapped with that of (calculated) pure InN for the photon energy beyond the s_1 shoulder. Moreover, a small reduction in s_1 shoulder of the N30/O5 spectrum in comparison with that of N30/O0 is nicely reproduced by the $InN_{0.6}O_{0.4}$ alloy simulation. The reduction in the s_1 shoulder can be attributed to the changes in the lowest conduction band states due to the replacement of N by O atoms. Note that a calculated spectrum based on a combination of fourfold and sixfold In (not shown) does not give such a good agreement. For samples with higher O contents (N30/O10 and N30/O20) the spectra show a mixed signature between that of fourfold and sixfold In atoms. The excess O atoms above the substitutional solubility limit (assumed to be ~40%) of InN can either form a phase separated In_2O_3-like structure or an inclusion of local In_2O_3-like structure both of which leads to a formation of sixfold In atoms. In this model, the composition in the sample can be written as $(InN_{0.6}O_{0.4})_F(InO_{1.5})_{1-F}$, where F is a fraction of fourfold In atoms out of all In atoms. The value of F can be calculated using a relationship $[O]:[In]=0.4F+1.5(1-F)$, where the [O]:[In] ratio of each sample was determined from AES and is shown in Table I. This gives the F values of 0.49 and 0.38 for N30/O20 and N30/O10, respectively. The corresponding spectra, which are calculated using weight averaged between $InN_{0.6}O_{0.4}$ and pure In_2O_3, are shown in Fig. 2(b). The spectra show the mixed signature of InN and In_2O_3 that are consistent with the measured spectra of N30/O10 and N30/O20. s_1 shoulder also further decreased from pure InN as more O content is added (insets of Fig. 2).

In a detail investigation, the spectra of both N30/O10 and N30/O20 samples appear to be very similar to each other and the s_1 shoulder of N30/O20 is only slightly lower than N30/O10 [see the inset of Fig. 2(a)]. The simulations also show the same trend, i.e., the s_1 shoulder of the spectrum with $F=0.38$ is just slightly lower than that of $F=0.49$ [see the inset of Fig. 2(b)]. However, when observing the decrease in s_1 shoulder in comparison to that of InN, we can see that the simulations ($F=0.38$ and $F=0.49$ spectra) give larger drop in the s_1 shoulder in comparison to those of samples N30/O10 and N30/O20. This suggests that N30/O10 and N30/O20 samples may contain more fourfold In atoms, i.e., higher F ratios, than those used in the simulations. We found that a simulation with $F\sim 2/3$, i.e., 2/3 of In atoms are fourfold and 1/3 of In atoms are sixfold, can provide a better agreement in the s_1 feature with the experiment (not shown). We speculate that there exist an intermediate crystal structure that have a fix number of fourfold In atoms and sixfold In atoms, in the unit cell. Although N atoms would prefer to decorate fourfold In atoms whereas O atoms would prefer sixfold In atoms, the interchanging of the anions is possible, leading to a very different optical properties in the two samples. Since the XANES signatures are not very sensitive to these anion interchanging, the spectra of the two samples remain very close. Further work is needed to settle down this issue.

In summary, we have performed In L_3-edge XANES study of indium oxynitride prepared by rf magnetron sputtering with different oxygen contents. The independent first principles XANES calculations of bulk InN and In_2O_3 give unambiguous agreement with the spectra from the samples prepared by using only N_2 and O_2 gas, respectively. Our results suggest that as much as 40% of oxygen can replace N in fourfold InN structure. The spectra from the samples with higher O contents show that the alloy contains both fourfold and sixfold indium atoms. This implies that either the samples are phase separated or there exist a preferred intermediate crystal structure containing both fourfold and sixfold In atoms. Our calculations also show that the XANES features are not strongly affected by the substitution of N by O or vice versa.

This work is supported by Commission on Higher Education, Thailand (CHE-RES-RG "Theoretical Physics"), the Thailand Research Fund (BRG5180001 and PHD/0107/2548), and AOARD/AFOSR (FA4869-08-1-4007). Work at KMITL is supported by NANOTEC, Thailand (CoE Network). S.L. thanks MRSEC Program of the NSF (DMR05-20415), NSF IMI (DMR 04-09848), SSLDC, and CNSI for supports and hospitality during his visit at UCSB, USA. We thank P. Songsiririthigul for useful discussions and W. Klysubun for facilitating x-ray measurements.

[1] J. Wu, W. Walukiewicz, S. X. Li, R. Armitage, J. C. Ho, E. R. Weber, E. E. Haller, H. Lu, W. J. Schaff, A. Barcz, and R. Jakiela, Appl. Phys. Lett. **84**, 2805 (2004).

[2] S.-H. Wei, X. Nie, I. G. Batyrev, and S. B. Zhang, Phys. Rev. B **67**, 165209 (2003).

[3] V. Yu. Davydov, A. A. Klochikhin, R. P. Seisyan, V. V. Emtsev, S. V. Ivanov, F. Bechstedt, J. Furthmuller, H. Harima, A. V. Mudryi, J. Aderhold, O. Semchinova, and J. Graul, Phys. Status Solidi B **229**, r1 (2002).

[4] J. Wu, W. Walukiewicz, K. M. Yu, J. W. Ager Iii, E. E. Haller, H. Lu, W. J. Schaff, Y. Saito, and Y. Nanishi, Appl. Phys. Lett. **80**, 3967 (2002).

[5] A. G. Bhuiyan, K. Sugita, K. Kasashima, A. Hashimoto, A. Yamamoto, and V. Y. Davydov, Appl. Phys. Lett. **83**, 4788 (2003).

[6] J. Wu, W. Walukiewicz, W. Shan, K. M. Yu, J. W. Ager, E. E. Haller, H. Lu, and W. J. Schaff, Phys. Rev. B **66**, 201403 (2002).

[7] V. Yu. Davydov, A. A. Klochikhin, V. V. Emtsev, S. V. Ivanov, V. V. Vekshin, F. Bechstedt, J. Furthmuller, H. Harima, A. V. Mudryi, A. Hashimoto, A. Yamamoto, J. Aderhold, J. Graul, and E. E. Haller, Phys. Status Solidi B **230**, r4 (2002).

[8] A. Klein, Appl. Phys. Lett. **77**, 2009 (2000).

[9] Motlan, E. M. Goldys, and T. L. Tansley, J. Cryst. Growth **241**, 165 (2002).

[10] M. Yoshimoto, H. Yamamoto, W. Huang, H. Harima, J. Saraie, A. Chayahara, and Y. Horino, Appl. Phys. Lett. **83**, 3480 (2003).

[11] Y. Yi, S. Cho, Y. Roh, M. Noh, C.-N. Whang, K. Jeong, and H.-J. Shin, Jpn. J. Appl. Phys., Part 1 **44**, 17 (2005).

[12] P. Fons, H. Tampo, A. V. Kolobov, M. Ohkubo, S. Niki, J. Tominaga, R. Carboni, F. Boscherini, and S. Friedrich, Phys. Rev. Lett. **96**, 045504 (2006).

[13] G. Ciatto, F. Boscherini, A. A. Bonapasta, F. Filippone, A. Polimeni, and M. Capizzi, Phys. Rev. B **71**, 201301 (2005).

[14] S. Limpijumnong, S. Rujirawat, A. Boonchun, M. F. Smith, and B. Cherdhirunkorn, Appl. Phys. Lett. **90**, 103113 (2007).

[15] N. Kietipaisalsophon, W. Bunjongpru, and J. Nukeaw, Int. J. Mod. Phys. B **16**, 4418 (2002).

[16] A. Sungthong, S. Porntheeraphat, A. Poyai, and J. Nukeaw, "An extreme change in structural and optical properties of indium oxynitride deposited by reactive gas-timing RF magnetron sputtering," Appl. Surf. Sci.

[17] G. Kresse and J. Furthmüller, Comput. Mater. Sci. **6**, 15 (1996).

[18] A. L. Ankudinov, C. E. Bouldin, J. J. Rehr, J. Sims, and H. Hung, Phys. Rev. B **65**, 104107 (2002).

[19] A. L. Ankudinov, B. Ravel, J. J. Rehr, and S. D. Conradson, Phys. Rev. B **58**, 7565 (1998).

[20] We calculated a supercell of InN with one N replaced by an O atom. The calculated XANES of In atom next to this O is almost indistinguishable from that of pure InN. Further test shows that even all four N neighbors are replaced by O atoms, the spectrum is still remarkably similar to the pure InN. Similarly, a replacement of one O by a N in In_2O_3 supercell gives ignorable change in the spectrum compared to pure In_2O_3. These tests clearly show that although the XANES features are sensitive to the structural arrangements of the neighbors of the In atom (fourfold or sixfold), they are not very sensitive to the interchanging of the anions.

PHYSICAL REVIEW B **77**, 195209 (2008)

Carbon-nitrogen molecules in GaAs and GaP

Sukit Limpijumnong,[1,2] Pakpoom Reunchan,[1,2] Anderson Janotti,[1] and Chris G. Van de Walle[1]
[1]*Materials Department, University of California, Santa Barbara, California 93106, USA*
[2]*School of Physics, Suranaree University of Technology and National Synchrotron Research Center, Nakhon Ratchasima 30000, Thailand*

(Received 6 February 2008; published 21 May 2008)

A carbon-nitrogen molecule in GaAs and GaP is investigated by using first-principles density functional pseudopotential calculations. The formation energy calculations show that the molecule favors substituting for an anion site (As or P) over being an interstitial under all equilibrium growth conditions. Under *p*-type conditions, the molecule exhibits the characteristic triple bonding and acts as a donor. When the Fermi level is higher (*n* type), the molecule acts as an acceptor by accepting electrons into its antibonding states and exhibits double or single bonding. The bond length and vibrational frequencies for each configuration are calculated and compared to those in recent experiments. Trends in the changes in bond length and vibrational frequencies with respect to the number of electrons in the antibonding states are discussed.

DOI: 10.1103/PhysRevB.77.195209 PACS number(s): 61.72.−y, 71.55.Eq

I. INTRODUCTION

Small amounts of nitrogen can strongly affect the electronic properties, such as the band gap and electron effective mass, of GaP and GaAs. This opens up an opportunity to continuously modify the band gap (as well as other properties) of these III–V semiconductors for advanced electronic and optoelectronic devices. This prospect has stimulated substantial research on dilute GaAsN and GaPN alloys both experimentally[1–7] and theoretically.[8–14] It is therefore very important that defects and impurities in these alloys are studied in detail. Carbon is a common impurity in various growth techniques[15,16] and sometimes, it is intentionally used as a *p*-type dopant;[17–20] complex formations between C and N could therefore be an important issue. Recently, Ulrici and Clerjaud[21] observed a sharp local vibration mode at 2087 cm^{-1} (at $T=7$ K) in GaP and a similar mode in GaAs. They identified it as a CN complex with a triple bond (between C and N) aligned along the [100] direction.

An experimental work[21] rigorously identified the chemical composition and the dipole direction of the complex; however, the actual location of the CN molecule in the lattice is still unclear. Both CN substituting on anion sites ($\mathrm{CN}_{\mathrm{As}}$ in GaAs or CN_{P} in GaP) and interstitial CN (CN_i) are potentially consistent with experiment and were proposed as possible models in Ref. 21. In other semiconductor compounds (such as ZnO, GaN, and ZnSe), small diatomic molecules such as N_2, O_2, or CN have been studied both by first-principles calculations and by different experiments and found to prefer substitution on an anion site.[15,22–25] However, the energy difference between the substitutional and interstitial sites varies from material to material; explicit calculations are therefore required to determine which site is more favorable for a given material.

In this paper, we use first-principles calculations to calculate the formation energies of $\mathrm{CN}_{\mathrm{As(or\ P)}}$ and CN_i. We find that, similar to other semiconductor compounds that have been studied before, CN energetically prefers substituting on anion sites of GaAs and GaP over interstitial sites in all thermal equilibrium growth conditions. We also calculate the vibrational frequency of the complex and find reasonable agreement with the measured value. The CN molecule behaves very similarly in GaAs and GaP, and therefore, we will focus our discussion on CN in GaAs. Numerical results will be reported for both GaAs and GaP.

II. COMPUTATIONAL METHOD

Our calculations are performed by using density functional theory with the local density approximation (LDA).[26] We use ultrasoft pseudopotentials,[27] as implemented in the VASP code.[28] The Ga 3*d* electrons are treated as valence electrons. The cutoff energy for the plane-wave basis set is 262 eV. We use a supercell with 64 atoms for the defect studies, and a $2\times2\times2$ shifted Monkhorst–Pack special *k*-point grid (Γ point not included) is employed for the Brillouin zone integration. The calculated GaAs lattice constant (5.60 Å, which is within 1% of the experimental value) is used. The electronic deep levels introduced by CN are examined by taking averages over the special *k* points. All the atoms are relaxed by minimization of the Hellmann–Feynman forces until all the forces are less than 0.05 eV/Å.

The formation energies of CN_i and $\mathrm{CN}_{\mathrm{As}}$ are defined, following Refs. 22 and 29, as

$$E_f(\mathrm{CN}_i^q) = E_{\mathrm{tot}}(\mathrm{CN}_i^q) - E_{\mathrm{tot}}(\mathrm{bulk}) - \mu_{\mathrm{C}} - \mu_{\mathrm{N}} + qE_F,$$

$$E_f(\mathrm{CN}_{\mathrm{As}}^q) = E_{\mathrm{tot}}(\mathrm{CN}_{\mathrm{As}}^q) - E_{\mathrm{tot}}(\mathrm{bulk}) - \mu_{\mathrm{C}} - \mu_{\mathrm{N}} + \mu_{\mathrm{As}} + qE_F, \tag{1}$$

where $E_{\mathrm{tot}}(D^q)$ is the total energy of the supercell with defect D in charge state q. $E_{\mathrm{tot}}(\mathrm{bulk})$ is the total energy of the supercell without a defect. μ_{C}, μ_{N}, and μ_{As} are the chemical potentials of a C atom, an N atom, and an As atom, respectively. For convenience, μ_{C} and μ_{As} are referenced to the energy of a C atom in diamond and an As atom in solid As, respectively. μ_{N} is referenced to the energy of an N atom in a free N_2 molecule. Growth conditions for GaAs are close to equilibrium, requiring that $\mu_{\mathrm{Ga}}+\mu_{\mathrm{As}}=\mu_{\mathrm{GaAs}}=-0.69$ eV (calculated GaAs heat of formation), where μ_{Ga} is a chemical potential of a Ga atom, which is referenced to the energy of a Ga atom in bulk Ga. E_F is the electron Fermi level with respect to the valence-band maximum (VBM).

The local vibrational mode frequencies of the molecules are calculated by using the so-called frozen phonon approach,[30] in which we followed a practical methodology described in Ref. 31. Because C and N atoms have similar masses, we equally displaced C and N to calculate the potential energy of stretching and compressing bonds. The mass of the oscillator is taken as the reduced mass:

$$\mu = \frac{m_C m_N}{m_N + m_C}, \tag{2}$$

where m_C and m_N are the masses of C and N atoms. We find that the (harmonic) stretching vibrational frequencies of the oscillator agree very well with a full dynamic matrix calculation with the matrix constructed by displacing each and every atom in the supercell one at a time in all three principal axes directions. A test calculation (on CN_{As}^{2+}) shows that the agreement between the full dynamic and reduced-mass results is better than 5 cm^{-1}. An important benefit of the reduced-mass calculation (besides a significant reduction in computational effort) is that it allows us to calculate the anharmonic part of the vibration, which we found to be on the order of 20 cm^{-1}. The potential energy is evaluated at seven values of displacements, with a maximum amplitude of up to 10% of the C-N equilibrium bond distance. To test the accuracy of the approach, we calculated the stretch frequency of a C-N mode in the HCN molecule and obtained the value of 2057 cm^{-1}, which is slightly smaller than the experimental value of 2089 cm^{-1}.[32] The calculated equilibrium C-N bond distance is fortuitously equal to the experimental value of 1.156 Å. The small underestimation in vibrational frequency, which is by 32 cm^{-1}, is expected to be systematic. Therefore, we have added the value of $\omega_{ER} = 32$ cm^{-1} to all of our calculated frequencies as a systematic correction.

III. RESULTS AND DISCUSSION

We investigated two forms of CN molecules in GaAs: at the substitutional As site and at the interstitial site. If initially the CN molecule is symmetrically placed at the As site (in the form of a split-interstitial configuration) with its principal axis aligned along the [100] direction, due to the symmetry, the orientation of the molecule will remain unchanged even when relaxation is allowed. The resulting symmetric configuration, CN_{As}(sym), is shown in Fig. 1(a). However, this orientation is not the lowest energy one for all charge states. Breaking the symmetry causes the molecule (in some charge states) to spontaneously rotate, without any barrier, into an asymmetric configuration [Fig. 1(b), CN_{As}(asym) in the 2+ charge state].

For an interstitial CN, there are two possible sites for the zinc-blende crystal: the tetrahedral interstitial sites surrounded by either Ga [T_d(Ga)] or As atoms [T_d(As)]. The calculations show that CN_i energetically prefers the T_d(Ga) site over the T_d(As) site. The T_d(Ga) site is surrounded by four Ga atoms in a tetrahedral configuration similar to the local structure surrounding a substitutional As lattice site. Again, if the molecule is initially placed in a high-symmetry orientation, CN_i(sym), the orientation remains fixed by symmetry, but breaking the symmetry can lead to rotation of the molecule into a lower-energy asymmetric configuration, CN_i (asym).

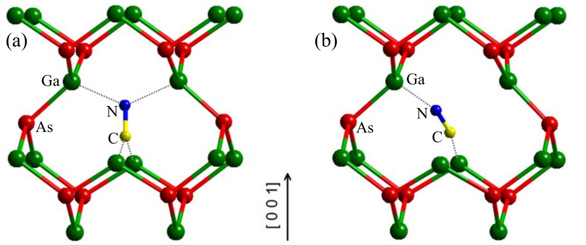

FIG. 1. (Color online) Local atomic geometry of a CN molecule substituting on an As site in GaAs: (a) symmetric configuration, CN_{As}(sym), and (b) asymmetric configuration, CN_{As}(asym). Both are shown for the 2+ charge state.

A. Substitutional CN molecules (CN_{As})

The substitutional molecule CN_{As} introduces a deep donor level (at approximately 0.25 eV) in the GaAs band gap, as shown in Fig. 2. The charge density (Fig. 3) of these levels resembles the $pp\pi^*$ molecular orbital of the CN molecule.[22] The molecular orbital theory tells us that the CN molecule has the following molecular orbitals, which are in order of increasing energy: $ss\sigma$, $ss\sigma^*$, $pp\pi$ (doublet), $pp\sigma$, $pp\pi^*$ (doublet), and $pp\sigma^*$. In the neutral charge state, the CN molecule on an As site has 12 valence electrons: 9 from the CN itself and 3 more contributed from the surrounding Ga atoms. These 12 electrons occupy the CN molecular orbitals up to the lower $pp\pi^*$ level and leave the higher $pp\pi^*$ level empty. Because the lower $pp\pi^*$ level is located deep inside the GaAs band gap, CN_{As} can donate up to two electrons and become CN_{As}^{2+} when the Fermi level of the system falls below the 0.25 eV donor level. The bonding between the C and N atoms in CN_{As}^{2+} is a triple bond ($C \equiv N$), with a bond distance of 1.17–1.20 Å (depending on the orientation), which is in good agreement with the known triple-bond length between C and N in HCN of 1.156 Å.[33]

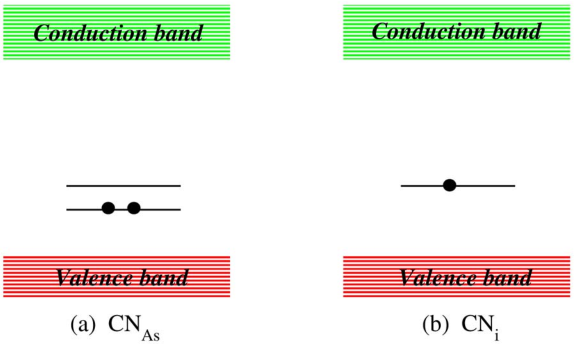

(a) CN_{As} (b) CN_i

FIG. 2. (Color online) Schematic illustrations of the $pp\pi^*$ single-particle energy levels of the CN molecule in the GaAs band gap. (a) Substituting on an As site (CN_{As}) and (b) CN on an interstitial site (CN_i). The solid dots show the electron occupation for the neutral charge state.

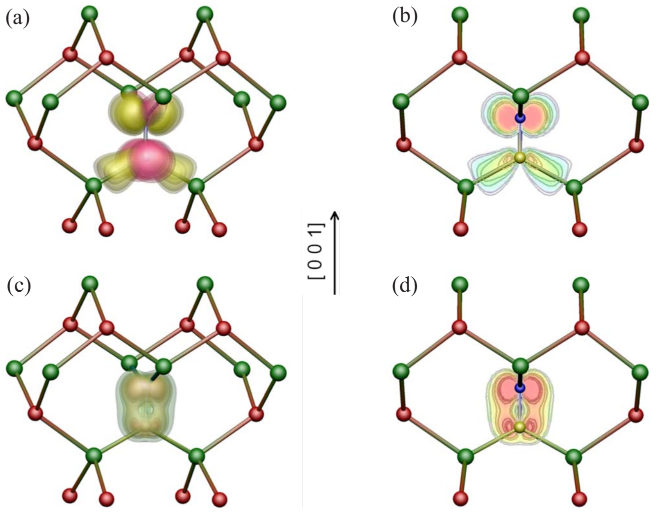

FIG. 3. (Color online) (a) Charge density of the $pp\pi^*$ states of CN_{As} that are located in the GaAs band gap. (b) Contour plot of one of the states in (a) in a (001) plane cutting through the CN molecule. (c) Charge density of one of the $pp\pi$ states of CN_{As} that resides below the valence-band maximum. (d) The corresponding contour plot of (c).

TABLE I. Calculated bond lengths $d_{\text{C-N}}$, stretching frequencies ω, and formation energies E_f (for the Fermi level at the VBM) of CN molecules in GaAs in the symmetric (asymmetric in parentheses) configurations. For each charge state, the lower-energy configuration is shown in boldface.

Charge state (q)	$d_{\text{C-N}}$ (Å)	ω (cm^{-1})	E_f (eV) Ga rich	E_f (eV) As rich
	CN on the As site (CN_{As})			
2+	1.20	1779	2.42	3.11
	(1.17)	**(2052)**	**(2.15)**	**(2.84)**
1+	**1.25**	**1481**	**2.42**	**3.11**
	(1.22)	(1734)	(2.46)	(3.15)
0	**1.30**	**1328**	**2.58**	**3.27**
	(1.25)	(1345)	(3.08)	(3.77)
1−	**1.35**	**1173**	**3.13**	**3.82**
	(1.31)	(1182)	(3.34)	(4.03)
2−	1.38	1095	4.03	4.72
	(1.40)	**(1097)**	**(3.82)**	**(4.51)**
	CN on the interstitial site (CN_i)			
1+	1.20	1897	4.41	4.41
	(1.19)	**(1934)**	**(3.85)**	**(3.85)**
0	**(1.25)**	**(1519)**	**(4.37)**	**(4.37)**

In the 2+ charge state, the $pp\pi^*$ level is unoccupied; hence, the CN_{As}^{2+} has little interaction with the surrounding neighbor. The molecule can therefore rotate quite freely, and it indeed moves away from the symmetric configuration to a new orientation that has a lower energy. Our calculated energy profile for the molecule rotating from the [001] to the (near) [110] direction, which is based on the nudged elastic band (NEB) method,[34] is shown in Fig. 4. We can see that starting from the symmetric [001] orientation, the molecule can rotate without any barrier to a new orientation in which the molecule's principal axis is nearly parallel with the [110] direction, lowering its energy by 0.27 eV in the process. By investigating the charge density (not shown), we found that the asymmetric configuration allows better interactions between the bonding pp states of CN and two of the surrounding Ga atoms, resulting in a lower formation energy.

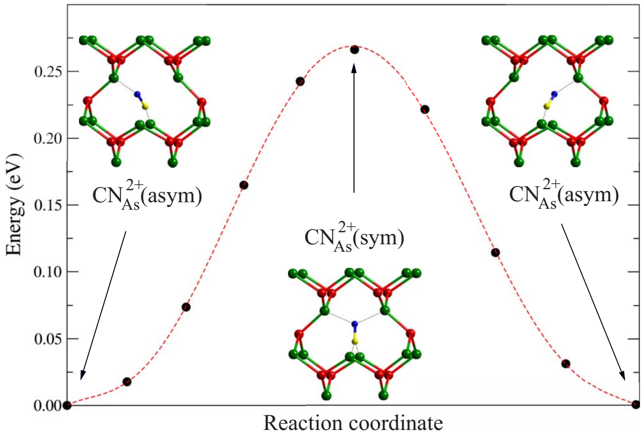

FIG. 4. (Color online) Calculated energy of CN_{As}^{2+} as the CN molecule rotates from the asymmetric to symmetric and back to an equivalent asymmetric configuration. The symmetric configuration is the saddle point along this path.

Starting from CN_{As}^{2+}, when the Fermi level is raised, the defect levels characteristic of $pp\pi^*$ molecular orbitals become occupied with electrons, and the charge state of CN_{As} increases from 2+ to 1+, 0, 1−, and 2−. Because these defect states correspond to antibonding orbitals of the free molecule, occupying them leads to an increase in the CN bond length (of approximately 0.05 Å per electron added), as shown in Table I. In addition, the charge density plots [Fig. 3(a) and 3(b)] reveal that the $pp\pi^*$ states hybridize with the dangling-bond states of the surrounding Ga atoms in the directions in which the density lobes are pointing. For instance, the lower two lobes in Fig. 3(b) clearly show the bond formation between the C atom and two Ga atoms, whereas the upper two lobes still maintain the molecular $pp\pi^*$ features. Because of the possibility of bond formation with the neighboring Ga atoms,CN_{As}^{1+}, CN_{As}^{0}, and CN_{As}^{1-} all favor the symmetric configuration.[35]

CN_{As}^{2-}, on the other hand, favors an asymmetric configuration (with a different orientation from that of CN_{As}^{2+}). Because the $pp\pi^*$ states are fully occupied, the molecule tries to optimize the Coulombic interaction between these $pp\pi^*$ states and its four Ga neighbors. Since the charge distribution for the CN molecule is not symmetric (the N atom is more electronegative than the C atom), the asymmetric configuration allows the N side of the molecule to bind with three Ga atoms instead of two, making the configuration more stable.

The formation energies of CN_{As} are shown in Table I (Table II for CN in GaP) and plots as a function of Fermi level are shown in Fig. 5 for two growth conditions: Ga rich ($\mu_{Ga}=0$) and As rich ($\mu_{As}=0$). As can be seen from Eq. (1),

TABLE II. Calculated bond lengths $d_{\text{C-N}}$, stretching frequencies ω, and formation energies E_f (for the Fermi level at the VBM) of CN molecules in GaP in the symmetric (asymmetric in parentheses) configurations. For each charge state, the lower-energy configuration is shown in boldface.

Charge state (q)	$d_{\text{C-N}}$ (Å)	ω (cm^{-1})	E_f (eV) Ga rich	E_f (eV) P rich
CN on the P site (CN$_P$)				
2+	1.20	1734	2.25	3.13
	(1.18)	**(2028)**	**(2.12)**	**(3.00)**
1+	**1.25**	**1517**	**2.40**	**3.28**
0	**1.31**	**1352**	**2.75**	**3.63**
1−	**1.36**	**1197**	**3.58**	**4.46**
	(1.33)	(1283)	(3.74)	(4.62)
2−	1.39	1113	4.77	5.65
	(1.41)	**(1105)**	**(4.50)**	**(5.38)**
CN on the interstitial site (CN$_i$)				
1+	1.21	1875	4.43	4.43
	(1.19)	**(1933)**	**(3.96)**	**(3.96)**
0	**(1.26)**	**(1511)**	**(4.82)**	**(4.82)**

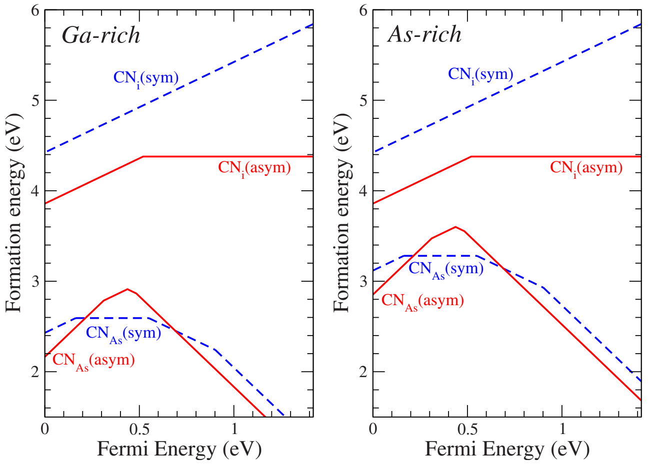

FIG. 5. (Color online) Formation energies of CN molecules in GaAs as a function of the Fermi energy. The solid lines and dashed lines represent the asymmetric and symmetric configurations, respectively.

the slope of the plot indicates the charge state of the CN molecule. In our plots, only the lowest energy charge state (at a given Fermi energy) is shown. For example, CN$_{\text{As}}$(asym) is stable in the 2+ charge state when the E_F of the system is located between 0.0 and 0.25 eV; therefore, the line has a slope of 2. For 0.25 eV$<E_F<$0.70 eV, the symmetric configuration becomes more stable and the neutral and 1− (for a narrow range near E_F=0.70 eV) charge states are the lowest in energy. At higher E_F, the asymmetric configuration with the 2− charge state, i.e., CN$_{\text{As}}^{2-}$(asym), becomes the most stable.[36] Therefore, the stable configurations in order of increasing E_F are as follows: CN$_{\text{As}}^{2+}$(asym), CN$_{\text{As}}^{0}$(sym), CN$_{\text{As}}^{1-}$(sym), and CN$_{\text{As}}^{2-}$(asym). CN$_{\text{As}}^{1+}$ is never stable. Because CN is substituting on the As site to form CN$_{\text{As}}$, its formation energy is lower in the Ga-rich condition than that in the As-rich condition. The plots also show that the formation energy of CN$_{\text{As}}$ is always lower than that of CN$_i$ for both the Ga- and As-rich conditions throughout the entire Fermi-energy range, with an energy difference of at least 1 eV. This implies that CN$_{\text{As}}$ is far easier to form than CN$_i$.

The trends in bonding discussed above are reflected in our calculated values of vibrational frequencies, which show that the frequency is highest for CN$_{\text{As}}^{2+}$ (2052 cm^{-1} for an asymmetric configuration and 1779 cm^{-1} for a hypothetical symmetric configuration). This is because in the 2+ charge state, the bonding states of the molecule are all occupied and the antibonding states ($pp\pi^*$) are all empty. As electrons are added into the antibonding states of CN$_{\text{As}}$, the C-N bond is weakened and the frequency is reduced to 1481, 1328, 1173, and 1097 cm^{-1} for CN$_{\text{As}}^{1+}$, CN$_{\text{As}}^{0}$, CN$_{\text{As}}^{1-}$, and CN$_{\text{As}}^{2-}$, respectively.

B. Interstitial CN molecules (CN$_i$)

The CN molecule has a total of nine electrons filling its molecular orbitals in the following order: $ss\sigma$, $ss\sigma^*$, $pp\pi$ (doublet), and with the last electron occupying $pp\sigma$. This leaves the $pp\sigma$ bonding state half-occupied and able to accept one more electron. Due to the strong bonding nature in the CN molecule, this $pp\sigma$ state has a low energy. When the molecule is placed in GaAs, the $pp\sigma$ state lies below the VBM and always becomes fully occupied. At the same time, the insertion of CN at an interstitial site also creates strain in nearby Ga-As bonds, leading to Ga-As bond extension (or breaking). The broken Ga-As bonds are shown in dotted lines in Fig. 6. CN$_i$ is stable in two charge states: 1+ and neutral. We initially used symmetric configurations in our calculations [Fig. 6(a)], but this configuration can spontaneously relax into asymmetric configurations with lower energies [Fig. 6(b) and 6(c)] if symmetry breaking is allowed. The energy change as the CN$_i$ rotates from the symmetric configuration into the asymmetric one (for 1+ charge state) calculated by using the NEB method is shown in Fig. 7. Figure 7 shows that the asymmetric configuration is favored

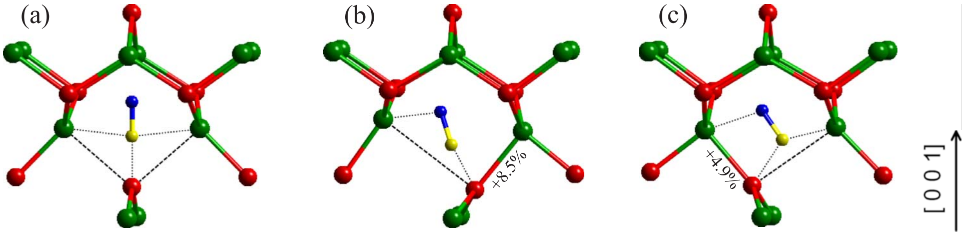

FIG. 6. (Color online) Local atomic geometry of interstitial CN molecules in GaAs: (a) CN$_i^+$(sym), (b) CN$_i^+$(asym), and (c) CN$_i^0$(asym).

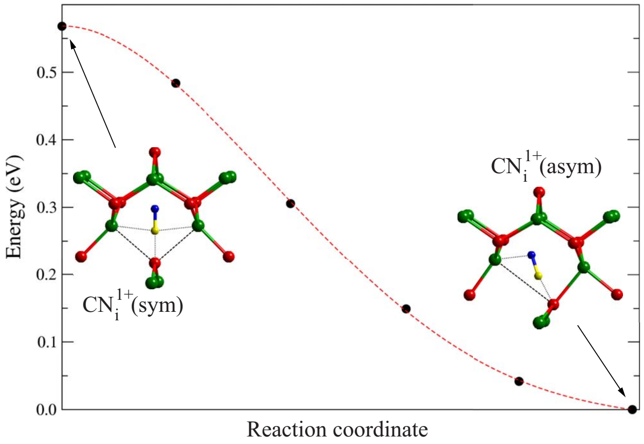

FIG. 7. (Color online) Calculated energy of CN_i^{1+} as the CN molecule rotates from a symmetric to an asymmetric configuration. The rotation occurs without any barrier and lowers the energy by almost 0.6 eV.

over the symmetric one by ~0.6 eV. We can clearly see in the asymmetric configuration [Fig. 6(c)] that only one of the Ga-As bonds is now broken (another bond is extended from a typical Ga-As bond). One of the two electrons released from the broken bond goes to the $pp\sigma$ state of the CN molecule, whereas another one is removed, resulting in the 1+ charge state. As an additional electron is added (increasing the charge state of the defect from 1+ to neutral), the additional electron goes to the $pp\pi^*$ level, which is located at approximately 0.5 eV above the VBM (see Fig. 2). This leads to the +/0 transition level of CN_i at 0.5 eV above the VBM. The occupation of the $pp\pi^*$ level leads to the increase in the CN bond to 1.25 Å and is reflected in an enhanced binding between the molecule and its neighbors [Fig. 6(c)] compared to the 1+ charge state [Fig. 6(b)}. Because the electron density of the $pp\pi^*$ state has four lobes pointing outward, which is similar to Fig. 3(b), when this state is occupied, the molecule can gain energy by turning the lobes to form bonds with the neighboring atoms.

Vibrational frequencies for the stretching modes of CN_i in GaAs and GaP are shown in Tables I and II. The frequency is higher for the CN_i in the 1+ charge state, which has all the bonding states occupied and the antibonding states empty. The frequency of 1934 cm^{-1} (1897 cm^{-1} for a hypothetical symmetric configuration) is comparable to that of CN_{As}^{2+}(asym), which has a similar electron occupation on the molecule. For the neutral charge state CN_i, with an electron occupying the $pp\pi^*$ state, the C-N bond length increases to 1.25 Å and the vibrational frequency decreases to 1519 cm^{-1}.

C. General trends of the bond length and the vibrational frequency

Our results show that the C-N bond distance becomes larger (and the vibrational frequency becomes lower) as more electrons are added into the $pp\pi^*$ states. Our investigations of the various configurations of CN molecules in GaAs and GaP allow us to quantitatively study the relationship between the electron occupation (of the CN molecule) and the bond length as well as the vibrational frequency. To do this, we define Δq as the additional charge being added to the CN molecule relative to the neutral free CN molecule. A free CN molecule has nine electrons, which occupy the molecular states up to half of the $pp\sigma$ state. Since this state is located below the VBM of GaAs, it is always fully occupied. This means that at least one electron from the host has to be added to the molecule ($\Delta q=-1$) and the electron occupation of the molecule becomes the same as that of a free (triple-bonded) CN^- ion. For the CN molecule in GaAs, this occupation corresponds to the lowest charge state, i.e., CN_{As}^{2+} and CN_i^{1+}. As the Fermi energy is raised, electrons are inserted into the antibonding states ($pp\pi^*$ states) of the CN molecule, thus weakening the C-N bond. When two electrons are inserted into the antibonding state (i.e., CN_{As}^0), making $\Delta q=-3$, the C-N bond is reduced to a double bond instead of a triple bond. When four electrons are inserted into the antibonding states (i.e., CN_{As}^{2-}), making $\Delta q=-5$, the C-N bond is reduced to a single bond. Our calculations thus show that CN_{As} can have its bond strength varied from a triple bond down to a single bond depending on the electron occupation. CN_i, on the other hand, can only exhibit the bond strength of a triple bond (CN_i^{1+}) or a triple bond with one electron in the antibonding state (CN_i^0) (which can be considered as halfway between a double bond and a triple bond).

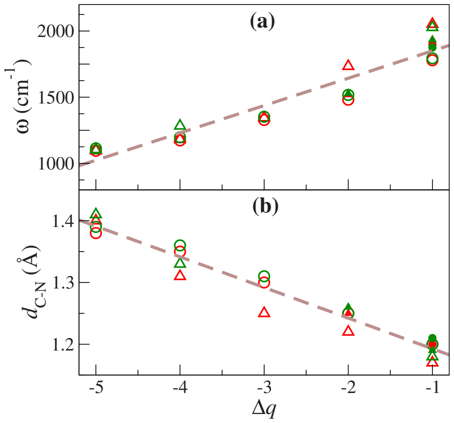

FIG. 8. (Color online) (a) Calculated vibrational frequencies and (b) C-N bond distances for various configurations of a CN molecule in GaAs and GaP as a function of charge Δq inserted into the molecule, which are measured relative to a neutral free CN molecule with nine electrons. The solid symbols are for interstitial CN and the open symbols are for substitutional CN. The colors code the host material (red for GaAs and green for GaP), whereas the symbols are used to distinguish the symmetric (circle) from the asymmetric (triangle) configurations. The CN molecule is characterized as triply, doubly, or singly bonded for $\Delta q=-1$, -3, and -5, respectively. The dashed lines are linear fits to all of the data points.

A plot of the C-N bond distance as a function of Δq is shown in Fig. 8(b). The bond distance, especially of the symmetric configurations, clearly show a linear trend with Δq. The deviations from the linear trend in the case of some of the asymmetric configurations can be attributed to the interaction with neighboring host atoms. A linear fit between the bond distance and Δq for all data points yields

$$d_{\text{C-N}} = -0.0496\Delta q + 1.143, \tag{3}$$

where $d_{\text{C-N}}$ is the bond distance between C and N in Å. The bond length increases by approximately 0.05 Å for every electron inserted.

The vibrational frequency decreases as the bond is extended. The relationship between the frequency and Δq is shown in Fig. 8(a). Again, a linear trend is seen. A linear fit yields

$$\omega = 207\Delta q + 2057, \tag{4}$$

where ω is the vibration frequency in cm^{-1}, i.e., the frequency is redshifted by approximately 200 cm^{-1} for every electron that is inserted. Deviations from the fit (on the order of 100 cm^{-1}) occur because the actual frequency also depends on other factors such as the detailed local geometry. Still, the linear fit in Eq. (4) nicely highlights the general trend, even if it does not provide a completely accurate prediction of the frequency.

D. Discussion and comparison with experiment

Ulrici and Clerjaud[21] performed a polarized infrared absorption spectroscopy on C-doped dilute-nitride GaAs and GaP. They observed a sharp local vibrational mode at 2087.1 cm^{-1} (at $T=7$ K) in GaP and a similar mode (2088.5 cm^{-1}) in GaAs. They identified it as a CN complex with a triple bond (between C and N) aligned along three equivalent ⟨100⟩ directions. Their C and N assignments were based on their observation of additional weak peaks at 2031 and 2048 cm^{-1}, which exhibit an intensity ratio and frequency shift that match the natural abundance and predicted frequency shift for C^{13} and N^{15} isotopes. The orientation of the molecule was confirmed by polarized IR absorption under different types of uniaxial stress.

An inspection of Tables I and II shows that the measured frequency of 2087 cm^{-1} is most consistent with our calculated frequencies for triply bonded CN molecules with $\Delta q = -1$. A more detailed identification runs into some complications, however. There are four configurations with triple bonds covered in our study: $\text{CN}_{\text{As}}^{2+}$(asym), $\text{CN}_{\text{As}}^{2+}$(sym), CN_i^{1+}(asym), and CN_i^{1+}(sym). (1) $\underline{\text{CN}_{\text{As}}^{2+}\text{(asym)}}$ provides the best matching frequency to the experiment (lower by 36 cm^{-1}, which is well within the computational error bar). However, the molecule does not align along ⟨100⟩ but, instead, prefers to align in a direction close to ⟨110⟩. (2) $\underline{\text{CN}_{\text{As}}^{2+}\text{(sym)}}$ has the correct orientation; however, its frequency is too low (by 309 cm^{-1}), and, even more importantly, it is not energetically stable and spontaneously rotates to $\text{CN}_{\text{As}}^{2+}$(asym), lowering the energy by 0.27 eV. Therefore, we can rule out $\text{CN}_{\text{As}}^{2+}$(sym). (3) $\underline{\text{CN}_i^{1+}\text{(asym)}}$ is a possible candidate. Its calculated vibrational frequency is not too far from the observed value (lower by 154 cm^{-1}). However, its orientation also deviated from ⟨100⟩ by 16°. In addition, the interstitial configurations are energetically unfavorable compared to those of $\text{CN}_{\text{As}}^{2+}$(asym). (4) $\underline{\text{CN}_i^{1+}\text{(sym)}}$ is an unlikely candidate because it is not energetically stable. It can spontaneously rotate to the asymmetric configuration and gain 0.6 eV. In addition, its vibrational frequency is even lower than that of the asymmetric configuration, widening the disagreement with experiment to 191 cm^{-1}.

Our first-principles calculations of vibrational frequencies for CN molecules in various configurations in GaAs and GaP therefore generally support Ulrici and Clerjaud's[21] assignment of the 2087 cm^{-1} mode to a triply bonded CN molecule. However, our calculations also show that the triply bonded CN molecule (in either the substitutional or interstitial configurations) does *not* symmetrically align in a tetrahedral site surrounded by four Ga atoms. As a result, neither CN_{As} nor CN_i have the C-N axis aligned in the ⟨100⟩ direction, as proposed by Ulrici and Clerjaud.[21] However, given a rather low rotation barrier of only 0.27 eV (Fig. 4), it is possible that $\text{CN}_{\text{As}}^{2+}$(asym) is constantly rotating, resulting in an average orientation in the ⟨100⟩ direction observed in the experiment.

IV. CONCLUSIONS

We have presented first-principles results for CN molecules in GaAs and GaP. The study covered two possible lattice locations: (1) CN molecules substituting for anions ($\text{CN}_{\text{As(or P)}}$) and (2) interstitial CN molecules at the T_d site surrounded by four Ga atoms (CN_i). All possible charge states and various orientations were considered. The calculated formation energies show that the molecule favors substituting for the anion site over the interstitial configuration for all equilibrium growth conditions with a margin of at least 1 eV. The calculations predict the CN molecule to produce a level with a strong $pp\pi^*$ molecular orbital characteristic at approximately 0.5–0.8 eV above the VBM. In p-type conditions, where the Fermi level is located below this $pp\pi^*$ level, the molecules are triply bonded and form donor defect centers (double donor $\text{CN}_{\text{As}}^{2+}$ and single donor CN_i^{1+}). The calculations with full relaxation show that triply bonded $\text{CN}_{\text{As}}^{2+}$ and CN_i^{1+} do not symmetrically orient in the Ga tetrahedron but, instead, are tilted in order to gain better interactions with neighboring Ga atoms. The calculated vibration frequencies of the triply boned $\text{CN}_{\text{As}}^{2+}$ and CN_i^{1+} are in reasonable agreement with the measurement by Ulrici and Clerjaud supporting their identification that the bonding is triple-bond type. Although neither CN_{As} nor CN_i have the C-N bond oriented along the ⟨100⟩ directions, as proposed by Ulrici and Clerjaud,[21] the low rotation barrier of $\text{CN}_{\text{As}}^{2+}$ makes it possible that the molecule might be constantly rotating, leading to an average orientation in the ⟨100⟩ direction. At higher Fermi levels, the CN_i^{1+} can accept an electron and becomes CN_i^{0}, whereas $\text{CN}_{\text{As}}^{2+}$ can accept one, two, three, or four electrons (depending on the Fermi level) and becomes $\text{CN}_{\text{As}}^{1+}$, $\text{CN}_{\text{As}}^{0}$ (metastable), $\text{CN}_{\text{As}}^{1-}$, or $\text{CN}_{\text{As}}^{2-}$, respectively. We found that the C-N bond length and vibrational frequency linearly change (to a good approximation) with the number of electrons added into the antibonding states of the molecule.

ACKNOWLEDGMENTS

This work was supported in part by the MRSEC Program of the National Science Foundation under Award No.

DMR05-20415, by the NSF IMI Program under Award No. DMR 04-09848, and by the UCSB Solid State Lighting and Display Center. This work also made use of the CNSI Computing Facility under NSF Grant No. CHE-0321368. S.L. and P.R. thank the Thailand Research Fund (Grants No. BRG5180001 and No. PHD/0203/2546), AOARD/AFOSR (Grant No. FA4869-08-1-4007), and the California NanoSystems Institute for the hospitality.

---

[1] K. M. Yu, W. Walukiewicz, J. Wu, D. E. Mars, D. R. Chamberlin, M. A. Scarpulla, O. D. Dubon, and J. F. Geisz, Nat. Mater. **1**, 185 (2002).

[2] W. Shan, W. Walukiewicz, J. W. Ager, E. E. Haller, J. F. Geisz, D. J. Friedman, J. M. Olson, and S. R. Kurtz, Phys. Rev. Lett. **82**, 1221 (1999).

[3] I. A. Buyanova, M. Izadifard, W. M. Chen, H. P. Xin, and C. W. Tu, Phys. Rev. B **69**, 201303(R) (2004).

[4] N. Q. Thinh, I. P. Vorona, I. A. Buyanova, W. M. Chen, S. Limpijumnong, S. B. Zhang, Y. G. Hong, C. W. Tu, A. Utsumi, Y. Furukawa, S. Moon, A. Wakahara, and H. Yonezu, Phys. Rev. B **70**, 121201(R) (2004).

[5] G. Pettinari, F. Masia, A. Polimeni, M. Felici, A. Frova, M. Capizzi, A. Lindsay, E. P. O'Reilly, P. J. Klar, W. Stolz, G. Bais, M. Piccin, S. Rubini, F. Martelli, and A. Franciosi, Phys. Rev. B **74**, 245202 (2006).

[6] G. Pettinari, A. Polimeni, F. Masia, R. Trotta, M. Felici, M. Capizzi, T. Niebling, W. Stolz, and P. J. Klar, Phys. Rev. Lett. **98**, 146402 (2007).

[7] G. Ciatto, F. Boscherini, A. A. Bonapasta, F. Filippone, A. Polimeni, and M. Capizzi, Phys. Rev. B **71**, 201301(R) (2005).

[8] P. R. C. Kent and A. Zunger, Phys. Rev. B **64**, 115208 (2001).

[9] M.-H. Du, S. Limpijumnong, and S. B. Zhang, Phys. Rev. Lett. **97**, 075503 (2006).

[10] M.-H. Du, S. Limpijumnong, and S. B. Zhang, Phys. Rev. B **72**, 073202 (2005).

[11] K. Kim and A. Zunger, Phys. Rev. Lett. **86**, 2609 (2001).

[12] A. M. Teweldeberhan and S. Fahy, Phys. Rev. B **72**, 195203 (2005).

[13] A. Amore Bonapasta, F. Filippone, and P. Giannozzi, Phys. Rev. B **68**, 115202 (2003).

[14] A. Janotti, S. B. Zhang, S.-H. Wei, and C. G. Van de Walle, Phys. Rev. Lett. **89**, 086403 (2002).

[15] X. Li, B. Keyes, S. Asher, S. B. Zhang, S.-H. Wei, T. J. Coutts, S. Limpijumnong, and C. G. Van de Walle, Appl. Phys. Lett. **86**, 122107 (2005).

[16] R. E. Welser, R. S. Setzko, K. S. Stevens, E. M. Rehder, C. R. Lutz, D. S. Hill, and P. J. Zampardi, J. Phys.: Condens. Matter **16**, S3373 (2004).

[17] W. Songprakob, R. Zallen, W. K. Liu, and K. L. Bacher, Phys. Rev. B **62**, 4501 (2000).

[18] K. H. Tan, S. F. Yoon, Q. F. Huang, R. Zhang, Z. Z. Sun, J. Jiang, W. Feng, and L. H. Lee, Phys. Rev. B **67**, 035208 (2003).

[19] J. R. L. Fernandez, F. Cerdeira, E. A. Meneses, M. J. S. P. Brasil, J. A. N. T. Soares, A. M. Santos, O. C. Noriega, J. R. Leite, D. J. As, U. Köhler, S. Potthast, and D. G. Pacheco-Salazar, Phys. Rev. B **68**, 155204 (2003).

[20] B.-H. Cheong and K. J. Chang, Phys. Rev. B **49**, 17436 (1994).

[21] W. Ulrici and B. Clerjaud, Phys. Rev. B **72**, 045203 (2005).

[22] S. Limpijumnong, X. N. Li, S. H. Wei, and S. B. Zhang, Appl. Phys. Lett. **86**, 211910 (2005).

[23] E.-C. Lee, Y. S. Kim, Y. G. Jin, and K. J. Chang, Phys. Rev. B **64**, 085120 (2001).

[24] P. Fons, H. Tampo, A. V. Kolobov, M. Ohkubo, S. Niki, J. Tominaga, R. Carboni, F. Boscherini, and S. Friedrich, Phys. Rev. Lett. **96**, 045504 (2006).

[25] A. Janotti and C. G. Van de Walle, Phys. Rev. B **76**, 165202 (2007).

[26] LDA provides a lattice constant of bulk GaP that is slightly in better agreement with that of experiment. On the other hand, generalized gradient approximation (GGA) provide a slightly better lattice constant for GaAs. Test calculations show that the choice of LDA/GGA only slightly affects the numerical value of energy and vibration frequency but does not change the main conclusions.

[27] D. Vanderbilt, Phys. Rev. B **41**, 7892 (1990).

[28] G. Kresse and J. Furthmüller, Comput. Mater. Sci. **6**, 15 (1996).

[29] S. B. Zhang and J. E. Northrup, Phys. Rev. Lett. **67**, 2339 (1991).

[30] J. Ashkenazi, Phys. Rev. B **26**, 1512 (1982).

[31] S. Limpijumnong, J. E. Northrup, and C. G. Van de Walle, Phys. Rev. B **68**, 075206 (2003).

[32] K. Kim and W. T. King, J. Chem. Phys. **71**, 1967 (1979).

[33] G. Herzberg, *Molecular Spectra and Molecular Structure: Electronic Spectra and Electronic Structure of Polyatomic Molecules* (Van Nostrand, New York, 1966).

[34] H. Jónsson, G. Mills, and K. W. Jacobsen, in *Classical and Quantum Dynamics in Condensed Phase Simulations*, edited by B. J. Berne, G. Ciccotti, and D. F. Coker (World Scientific, Singapore, 1998), p. 385.

[35] $\mathrm{CN}_{\mathrm{AS}}$ in the +1 and 0 charge states is stable in the symmetric configuration. Test calculations for 1+ showed that a dimer initially tilted by as much as 15° away from the symmetric direction, i.e., the [001] direction, spontaneously rotated back after relaxations. The asymmetric configurations are only metastable. The (higher-energy) metastable asymmetric configuration for each charge state is found by initially aligning the CN molecule along the [110] direction and allowing relaxation of its neighbors before letting the molecule itself relax. The metastable asymmetric configurations are higher in energy than the symmetric ones by 0.1 and 0.5 eV for the 1+ and neutral charge states, respectively. The dimer qualitatively behaves the same in GaP except that none of the metastable asymmetric configurations exists.

[36] Although the calculated LDA band gap (at the Γ point) for GaAs is only 0.6 eV, our calculations are performed at special k points wherein the lowest conduction band occurs at 1.08 eV above the VBM. Any defect levels that lie below 1.08 eV are therefore accounted for and can be properly occupied.

PHYSICAL REVIEW B **78**, 113203 (2008)

Hydrogen in ZnO revisited: Bond center versus antibonding site

Xian-Bin Li,[1] Sukit Limpijumnong,[2,3,*] Wei Quan Tian,[4] Hong-Bo Sun,[1] and S. B. Zhang[1,2,5]
[1]*State Key Laboratory on Integrated Optoelectronics, College of Electronic Science and Engineering, Jilin University, Changchun 130012, People's Republic of China*
[2]*National Renewable Energy Laboratory, Golden, Colorado 80401, USA*
[3]*School of Physics, Suranaree University of Technology and National Synchrotron Research Center, Nakhon Ratchasima 30000, Thailand*
[4]*State Key Laboratory of Theoretical and Computational Chemistry, Institute of Theoretical Chemistry, Jilin University, Changchun 130023, People's Republic of China*
[5]*Department of Physics, Applied Physics, and Astronomy, Rensselaer Polytechnic Institute, Troy, New York 12180, USA*
(Received 13 August 2008; published 15 September 2008)

Current controversy on the binding sites of H^+ in ZnO can be explained by first-principles calculations. Previous infrared measurements from different groups indicate different H sites, either at the bond center (BC) site with a stretch frequency $\omega = 3611\ \text{cm}^{-1}$ or antibonding (AB) site with $\omega = 3326\ \text{cm}^{-1}$. This was puzzling because the BC site has lower energy by 0.2 eV. Here, we show that calcium, isovalent to Zn and found only in samples with the $3326\ \text{cm}^{-1}$ mode, binds H at the AB site. Large spatial undulation of charge explains the unexpected large binding between isovalent Ca and charged H^+ of 0.7 eV.

DOI: 10.1103/PhysRevB.78.113203 PACS number(s): 61.72.Bb, 63.20.Pw

Hydrogen in ZnO has attracted a lot of attention in the last decade. In 2000, Van de Walle proposed that H prefers to form a strong O-H bond with lattice O and acts exclusively as a donor, H^+.[1] This behavior is different from H in almost all other semiconductors in which H is amphoteric, counteracting the dominant dopant.[2] ZnO is a potential superior electronic material for next-generation blue optoelectronic applications. However, due to the lacking of high quality *p*-type samples, fabrication of ZnO-based optoelectronic devices is still not possible. The prediction that H is an exclusive donor stirred up considerable research activities because it may explain the difficulty in *p* doping.[3–11]

Binding site is one of the most fundamental properties of any impurity. Although it is clear that H^+ prefers to bind strongly with O at a bond length of approximately 1 Å and with a vibration frequency around $3500\ \text{cm}^{-1}$, the details is completely controversial: McCluskey *et al.*[6] observed an IR peak at $3326\ \text{cm}^{-1}$ in samples provided by Cermet, while Lavrov *et al.*[12] observed a different peak at $3611\ \text{cm}^{-1}$ in samples by Eagle-Picher. Polarized IR showed that the $3326\ \text{cm}^{-1}$ peak is associated with an oscillator orientated at 112° angle with respect to the *c* axis, whereas those that give the $3611\ \text{cm}^{-1}$ peak are parallel to the axis. Later study by Shi *et al.*[7] on both samples showed that the Cermet samples have a strong $3326\ \text{cm}^{-1}$ peak and a weak $3611\ \text{cm}^{-1}$ peak but the Eagle-Picher samples do exactly the opposite. This indicates that there exist two forms of O-H in these two types of samples. Because the splitting $3611-3326=285\ \text{cm}^{-1}$ is comparable to the calculated splitting between the BC and AB site adjacent to O (AB_O), the $3611\ \text{cm}^{-1}$ peak has been assigned to $BC_\parallel$ and the $3326\ \text{cm}^{-1}$ peak to $AB_{O\perp}$,[13] where $\parallel$ and $\perp$ denote the orientation of the O-H bond with respect to the *c* axis [see Fig. 1(a)].

However, independent calculations by different groups[12,13] showed consistently that the $BC_\parallel$ site has lower formation energy than any other site by 0.2 eV, which, in comparison with the experimental temperature of 4 K, is quite large. More importantly, it is difficult to understand why the $AB_{O\perp}$ configuration can dominate in some samples but not in others. An alternative explanation is that one (or both) of the signals may come from an H complex rather than just an isolated H^+. Recently, McCluskey and Jokela[14] studied the trace-amount elements in both samples by using delayed gamma neutron activation analysis (DGNAA) and secondary-ion mass spectrometry (SIMS). They found that the Cermet samples, grown by a pressurized melt-growth

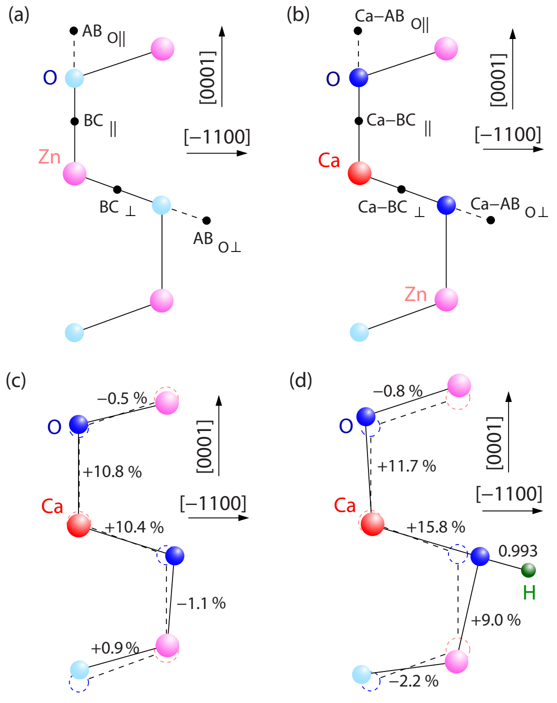

FIG. 1. (Color online) [(a) and (b)] Schematics in the (11−20) plane of the four H^+ sites in Ca-free ZnO and near a Ca impurity. Calculated atomic relaxations of Ca-$AB_{O\perp}$ (c) in the absence and (d) in the presence of H^+. Oxygen atoms adjacent to the Ca are marked by darker blue. Dashed circles and dashed lines indicate the original bulk positions and bonds. Distances are given either in unit of angstrom or in percentage with respect to that of bulk ZnO.

1098-0121/2008/78(11)/113203(4)

TABLE I. Calculated formation energy, O-H bond length, and stretch frequencies for H^+ in ZnO without (upper panel) and with (lower panel) Ca. The energy zero is that of Ca-free $BC_{\parallel}$ site. Highlighted rows are the ground-state configurations.

	ΔE(eV)		$d_{\text{O-H}}$ Å		Vibration frequency, $\omega(\text{cm}^{-1})$		
Site	Present	Ref. 13	Present	Ref. 13	Present	Ref. 13	Measured
$BC_{\parallel}$	**0.00**	**0.00**	**0.985**	**0.986**	**3421**	**3475**	**3611**[a]
$BC_{\perp}$	0.14	0.15	0.985	0.982	3505	3519	
$AB_{O\parallel}$	0.19	0.17	1.001	1.003	3097	3116	
$AB_{O\perp}$	0.15	0.14	1.004	1.003	3109	3154	
Ca-$BC_{\parallel}$	0.54		0.967		3934		
Ca-$BC_{\perp}$	0.38		0.979		3484		
Ca-$AB_{O\parallel}$	−0.29		0.995		3236		
Ca-$AB_{O\perp}$	**−0.49**		**0.993**		**3207**		**3326**[b]

[a] Reference 12.

[b] Reference 6.

process,[15] contain isovalent Ca impurity, whereas in the Eagle-Picher samples, which were grown by chemical vapor transport,[16] the amount of Ca impurity is below the detection threshold.

In this Brief Report, we show that Ca may play a pivotal role in switching the H from the $BC_{\parallel}$ site to the $AB_{O\perp}$ site. Our calculation shows that, with Ca, the $AB_{O\perp}$ site is 0.5 eV more stable than the ground-state $BC_{\parallel}$ site in pure, Ca-free ZnO. Our results are consistent with the experimental finding that, for Cermet samples with Ca, the 3326 cm^{-1} line is observed with the transition moment aligned at 112° from the c axis, whereas for Eagle-Picher samples without Ca, the 3611 cm^{-1} line with a transition moment aligned along the c axis is observed. The fact that an isovalent impurity can bind H^+ so strongly by $0.5+0.2=0.7$ eV is unexpected and hence surprising. Our analysis shows that this could be a general property of ionic semiconductors and solids for which the electrostatic monopole (such as H^+) and dipole (due to spatial undulated local field) interactions can be comparable to the monopole-monopole interactions (such as within a donor-acceptor pair) in more covalent materials.

We used the density-functional theory[17] within the local-density approximation (LDA) and the projector augmented wave method[18,19] as implemented in the VASP code.[20,21] Zinc 3d states are treated as valence states. The cut-off energy for the plane-wave expansion is 400 eV. We used a supercell approach (96-atom wurtzite cell) with the Monkhorst-Pack k-point mesh for the Brillouin-zone integration $(2\times2\times2)$. For charged defect, we used the jellium background approximation. All the atoms are allowed to relax to their equilibrium positions. To calculate the O-H frequencies, we employed the approach in Ref. 13 to include anharmonic effects. For free H_2O molecule, this yields a symmetric stretch frequency of 3540 cm^{-1}, which is lower than experiment[22] by $\omega_{ER}=117$ cm^{-1} (an error of ~3%). To correct such a systematic error, ω_{ER} has been added to all the calculated results before comparing with experiments.

Table I shows the calculated formation energies ΔE [relative to the ground-state ($BC_{\parallel}$) energy in Ca-free ZnO], O-H bond lengths $d_{\text{O-H}}$, and stretch frequencies ω for H^+ in ZnO without Ca (upper panel) and with Ca (lower panel). To be consistent, the upper panel are the results of current 96-atom cell calculations, which are qualitatively the same as previous calculations, e.g., $d_{\text{O-H}}$ and ω agree with our previous results to within 1% and 3%, respectively.[13] With Ca, we denote the complexes as Ca-$BC_{\parallel}$, Ca-$BC_{\perp}$, Ca-$AB_{O\parallel}$, and Ca-$AB_{O\perp}$, respectively, with their atomic structures schematically shown in Fig. 1(b). The formation energies of the Ca-containing complexes are defined as

$$\Delta E = E_{\text{tot}}(\text{Ca}-\text{H}^+) + E_{\text{tot}}(\text{bulk}) - E_{\text{tot}}(\text{Ca}_{\text{Zn}}) - E_{\text{tot}}(\text{BC}_{\parallel}), \tag{1}$$

where $E_{\text{tot}}(\alpha)$ is the total energy of a supercell containing the complex (or impurity) α. Physically, ΔE is the energy gain or loss by bringing a H^+ from the lowest-energy $BC_{\parallel}$ site in Ca-free ZnO to the respective sites near the Ca in Fig. 1(b). A negative ΔE implies that the H^+ is bounded, whereas a positive ΔE implies that the H^+ is unbounded, to the Ca. Even when ΔE is positive, the site is still metastable due to the diffusion barriers of H^+ in ZnO.

As Ca is *isovalent* to Zn, on a first look, it is puzzling why a charged H^+ would like to bind to a neutral Ca with a rather sizable energy—a behavior usually found either in oppositely charged donor-acceptor pairs or in charge neutral but large-strain compensated defect pairs. Our calculation shows that both substitutional Ca and interstitial H^+ cause outward relaxations to the surrounding Zn and O atoms. Therefore, neither of the above can be the cause for the unusually large binding energy. It is even more puzzling why the site preference is reversed from the BC site to the AB_O sites.

To understand the puzzles, we note first that H^+ in ZnO binds to the oxygen atoms rather than any of the cation atoms. Second, ZnO is a highly ionic semiconductor with an ionicity of 0.616 in Phillips' scale.[23] In other words, although ideal ZnO is a homogeneous bulk material, there is a large spatial undulation of the electric field at the atomic level. Therefore, the defect and impurity physics that is already well established for covalent semiconductors such as Si or GaAs may not necessarily apply here. Rather, it is how much

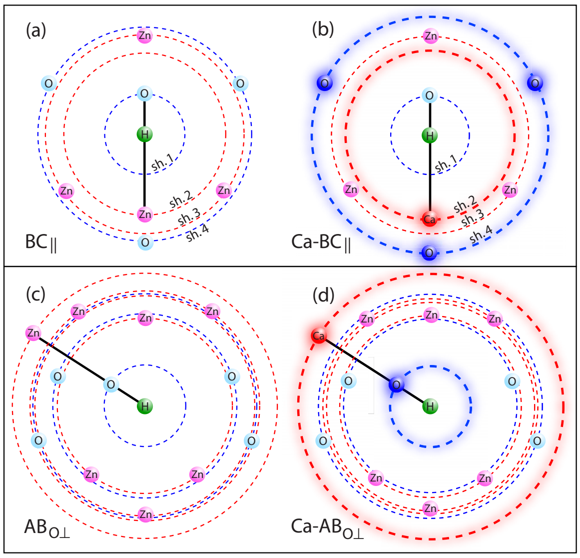

FIG. 2. (Color online) Radial distributions of neighboring atoms surrounding an H^+ at different sites: (a) $BC_\parallel$, (b) Ca-$BC_\parallel$, (c) $AB_{O\perp}$, and (d) Ca-$AB_{O\perp}$. Solid lines highlight the local bonds: O-H-Zn (or O-H-Ca) for the BC sites and H-O-Zn (or H-O-Ca) for the AB_O sites. Dashed circles indicate the radial distances from the H^+ center. For simplicity, atoms in the shell are evenly distributed. In (b) and (d), shells with enhanced charge with respect to (a) and (c) are highlighted by halo: blue for enhanced negative and red for enhanced positive.

the impurity affects the undulation of the field that holds the key to defect and impurity physics in ionic semiconductors. The electronegativity of Ca, Zn, and O, on the Pauling scale, is $\chi^{Ca}=1.00$, $\chi^{Zn}=1.65$, and $\chi^{O}=3.44$. Therefore, Ca has a stronger tendency to donate its electrons to neighboring O atoms than Zn does. This stronger charge transfer makes the O atoms adjacent to the Ca atom stronger negative centers relative to other O atoms. As such, qualitatively speaking, the H^+ should bind to these O atoms more strongly. Also, because Ca is a much stronger positive charge center than Zn, a H^+ would avoid the BC sites adjacent to Ca, making the adjacent AB_O sites energetically more favorable.

To further the discussion, next we apply a Bader analysis.[24,25] Our calculations show that in bulk ZnO, each Zn donates 1.13 electrons to O. In other words, Zn can be considered as a positive center with $q=+1.13e$ whereas O can be considered as a negative center with $q=-1.13e$. This explains why an H^+ prefers to stay close to the O, instead of Zn. Bader analysis of Ca_{Zn} further shows that Ca donates $1.42e$, which is $0.29e$ more than what Zn does. The extra donation is almost equally distributed among the four O nearest neighbors: $0.06e$ to the O in the [0001] direction, and $0.07e$ to each of the remaining three O.

To understand the switching in site preference from BC in bulk ZnO to AB_O near Ca_{Zn}, we need to examine next-nearest neighbors (~2 Å) where the difference between the BC and AB_O sites can be readily seen. Figure 2 shows, in a schematic shell model, the radial distributions of neighboring atoms of H. It so happens that before introducing the Ca, the four sites in the upper panel of Table I, $BC_\parallel$, $BC_\perp$, $AB_{O\parallel}$, and $AB_{O\perp}$, have reasonably close formation energies to within 0.2 eV. This enables us to interpret the changes upon Ca substitution primarily in terms of a *redistribution* of the charge. Because the BC sites are closer to the Ca [e.g., Fig. 2(b)], they become energetically unfavorable. In contrast, the AB_O sites are much further away from the Ca [see, Fig. 2(d)]. As a result, the AB_O sites benefit more from the charge redistribution, forming a stronger O-H^+ bond yet staying away from the positive Ca so as not to be strongly affected by it. Moreover, because H in the BC sites cuts the Ca-O bonds, it effectively blocks charge transfer from Ca to O. As a matter of fact, Bader charge on the first shell O atom in Fig. 2(b) is the same as the Ca-free case. Hence, not only does the Ca-BC sites become less favorable than the Ca-AB_O sites, the formers are positive in energy with respect to the $BC_\parallel$ site away from the Ca. In other words, H^+ will not bind to the Ca at the Ca-BC sites.

Next, we estimate the equilibrium distribution of H^+ among the various lattice sites α. By constructing the partition functions, we can derive the equations relating the concentration of $H^+(\alpha)$, $[H^+(\alpha)]$, to the overall chemical potential of H^+, μ_{H^+}.[26] Because we consider only H^+, Fermi-level dependence of the various sites α is the same. Vibrational energy contributions for these sites are similar, as well. Their contributions can thus be expressed as E_0 and

$$\tilde{\mu}_{H^+} = \mu_{H^+} - E_0 = \Delta E(\alpha) + kT \ln\left\{\frac{[H^+(\alpha)]}{j(n(\alpha)-[H^+(\alpha)])}\right\}, \qquad (2)$$

where $\Delta E(\alpha)$ is the formation energy of $H^+(\alpha)$ in Table I, $n(\alpha)$ is the density of available lattice sites for a specific $H^+(\alpha)$, and j is the number of symmetry degeneracy. For example, for H^+ at $BC_\parallel$ site, we have $\mu_{H^+}=0.0\ \text{eV}+kT\ln\{[H^+(BC_\parallel)]/[O]-[H^+(BC_\parallel)]\}$, and for H^+ at Ca-$AB_{O\perp}$ site, we have $\tilde{\mu}_{H^+}=-0.49\ \text{eV}+kT\ln([H^+(\text{Ca-}AB_{O\perp})]/3\{[Ca]-[H^+(\text{Ca-}AB_{O\perp})]\})$. To solve the set of equations, we apply the equilibrium constraint that $\tilde{\mu}_{H^+}$ is the same for all the $H^+(\alpha)$. We also require that the total concentration of H^+ satisfies $[H^+]=\Sigma[H^+(\alpha)]$, whose value is an input from experimental conditions.

For Cermet samples, the concentration of Ca is measured to be $[Ca]=4\times10^{16}\ \text{cm}^{-3}$ (Ref. 14) and the total concentration of H^+ is expected to be at most in the same order of magnitude (so we use $[H^+]=4\times10^{16}$ for the illustration purpose). Figure 3(a) shows the normalized equilibrium concentrations as a function of temperature. Concentrations with less than 5% of total $[H^+]$ are ignored in the figure. We see that the majority (over 75%) of H^+ is on the Ca-$AB_{O\perp}$ sites for temperatures below 400 K (or 127 °C). It has been predicted that H^+ diffuses readily at room temperature due to its low migration barrier of less than 0.5 eV (Refs. 3 and 27) to equilibrate the H^+ among the various lattice sites. For Eagle-Picher samples, the concentration of Ca is outside experimental detection limit and is hence much less than that of H^+. Figure 3(b) shows the results for such a case. Here as expected, the majority (over 75%) of H^+ is on the $BC_\parallel$ sites for temperatures less than 600 K.

The calculated vibrational signatures of the H^+ sites are also in agreement with experiments. For example, the stretch

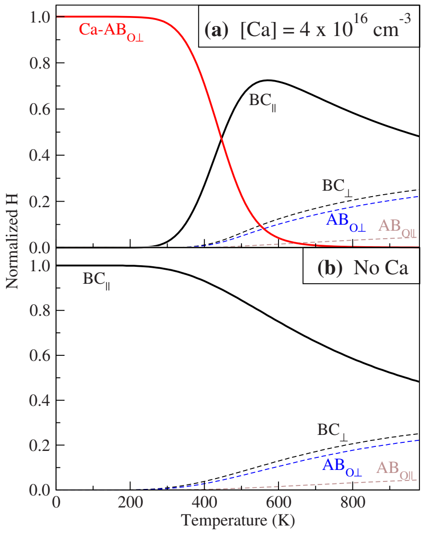

FIG. 3. (Color online) Normalized equilibrium concentrations of $[H^+(\alpha)]$ at the various sites α as a function of temperature. (a) is the case when $[Ca]=4\times10^{16}$ cm^{-3} and (b) is the case when there is no Ca. A total $[H^+]=4\times10^{16}$ cm^{-3} was assumed in the calculations.

frequencies of 3421 cm^{-1} for BC$_{\parallel}$ and 3207 cm^{-1} for Ca-AB$_{O\perp}$ agree, within computational uncertainty, with the experimental lines at 3611 (Eagle-Picher) and 3326 cm^{-1} (Cermet). Note that although the absolute values here differ from experiments by about 100–200 cm^{-1}, the difference between the two experimental modes of $3611-3326=285$ cm^{-1} is in a good agreement with that between the BC and AB$_O$ configurations of $3421-3207=214$ cm^{-1}. The BC$_{\parallel}$ configuration has the oscillator oriented along the *c* axis, which is consistent with the experimental observation for the Eagle-Picher samples. The Ca-AB$_{O\perp}$ configuration has the oscillator orientated at 107° with respect to the *c* axis, which is consistent with the polarized IR measurement for the Cermet samples with transition moment aligned at 112°.

In conclusion, the large atomic-level spatial undulation of electric field makes the defect and impurity physics in ionic materials, in particular in ZnO, qualitatively different from that of covalent semiconductors. Larger than expected binding energy of 0.7 eV can result between charge neutral, isovalent Ca, and H$^+$ impurities. This tilts the energy balance between the BC and AB$_O$ sites to favor AB$_{O\perp}$ in the presence of Ca. The calculated vibrational signatures of H$^+$ are also consistent with IR measurements. This may explain the current puzzle about the H$^+$ sites in ZnO.

This work was supported by NSFC (Contract No. 60525412), U.S. DOE/BES (Contract No. DE-AC36-99GO10337), JLU (start-up fund), CHE (CHE-RES-RG program), and AOARD/AFOSR (Contract No. FA4869-08-1-4007). We thank D. J. West, Z. G. Chen, X. Meng, H. Wang. D. Han, Q. D. Chen, and H. Yang for helpful discussios and technical supports.

---

*Corresponding author. sukit@sut.ac.th

[1] C. G. Van de Walle, Phys. Rev. Lett. **85**, 1012 (2000).
[2] C. G. Van de Walle and J. Neugebauer, Nature (London) **423**, 626 (2003).
[3] K. Ip, M. E. Overberg, Y. W. Heo, D. P. Norton, S. J. Pearton, C. E. Stutz, B. Luo, F. Ren, D. C. Look, and J. M. Zavada, Appl. Phys. Lett. **82**, 385 (2003).
[4] S. J. Jokela and M. D. McCluskey, Phys. Rev. B **72**, 113201 (2005).
[5] E. V. Lavrov and J. Weber, Phys. Rev. B **73**, 035208 (2006).
[6] M. D. McCluskey, S. J. Jokela, K. K. Zhuravlev, P. J. Simpson, and K. G. Lynn, Appl. Phys. Lett. **81**, 3807 (2002).
[7] G. A. Shi, M. Stavola, S. J. Pearton, M. Thieme, E. V. Lavrov, and J. Weber, Phys. Rev. B **72**, 195211 (2005).
[8] K. Shimomura, K. Nishiyama, and R. Kadono, Phys. Rev. Lett. **89**, 255505 (2002).
[9] S. F. J. Cox, E. A. Davis, S. P. Cottrell, P. J. C. King, J. S. Lord, J. M. Gil, H. V. Alberto, R. C. Vilão, J. Piroto Duarte, N. Ayres de Campos, A. Weidinger, R. L. Lichti, and S. J. C. Irvine, Phys. Rev. Lett. **86**, 2601 (2001).
[10] C. H. Seager and S. M. Myers, J. Appl. Phys. **94**, 2888 (2003).
[11] M. D. McCluskey and S. J. Jokela, *Proceedings of the NATO Advanced Workshop on Zinc Oxide*, NATO Science Series II: Mathematics, Physics, and Chemistry Vol. 194, edited by N. Nickel and E. Terukov (Springer, Dordrecht, 2005), p. 125.
[12] E. V. Lavrov, J. Weber, F. Börrnert, C. G. Van de Walle, and R. Helbig, Phys. Rev. B **66**, 165205 (2002).
[13] S. Limpijumnong and S. B. Zhang, Appl. Phys. Lett. **86**, 151910 (2005).
[14] M. D. McCluskey and S. J. Jokela, Physica B (Amsterdam) **401-402**, 355 (2007).
[15] D. C. Reynolds, C. W. Litton, D. C. Look, J. E. Hoelscher, B. Claflin, T. C. Collins, J. Nause, and B. Nemeth, J. Appl. Phys. **95**, 4802 (2004).
[16] R. Triboulet, V. Munoz-Sanjose, R. Tena-Zaera, M. C. Martinez-Tomas, and S. Hassani, *Proceedings of the NATO Advanced Workshop on Zinc Oxide*, NATO Science Series II: Mathematics, Physics, and Chemistry, Vol. 194, edited by N. Nickel and E. Terukov, (Springer, Dordrecht, 2005), p. 3.
[17] W. Kohn and L. J. Sham, Phys. Rev. **140**, A1133 (1965).
[18] P. E. Blöchl, Phys. Rev. B **50**, 17953 (1994).
[19] G. Kresse and D. Joubert, Phys. Rev. B **59**, 1758 (1999).
[20] G. Kresse and J. Furthmüller, Phys. Rev. B **54**, 11169 (1996).
[21] G. Kresse and J. Furthmuller, Comput. Mater. Sci. **6**, 15 (1996).
[22] E. McCartney, *Absorption and Emission by Atmospheric Gases: The Physical Processes* (Wiley, New York, 1983).
[23] J. C. Phillips, Rev. Mod. Phys. **42**, 317 (1970).
[24] R. F. W. Bader, *Atoms in Molecules: A Quantum Theory* (Oxford University Press, New York, 1994).
[25] G. Henkelman, A. Arnaldsson, and H. Jonsson, Comput. Mater. Sci. **36**, 354 (2006).
[26] A. F. Wright and S. M. Myers, J. Appl. Phys. **94**, 4918 (2003).
[27] M. G. Wardle, J. P. Goss, and P. R. Briddon, Phys. Rev. Lett. **96**, 205504 (2006).

Unexpected Coulomb binding between Ca and H^+ in ZnO

Xian-Bin Li[a)]
State Key Laboratory on Integrated Optoelectronics, College of Electronic Science and Engineering, Jilin University, Changchun 130012, China

Sukit Limpijumnong
School of Physics, Suranaree University of Technology, Nakhon Ratchasima 30000, Thailand and Synchrotron Light Research Institute, Nakhon Ratchasima 30000, Thailand

Wei Quan Tian
State Key Laboratory of Theoretical and Computational Chemistry, Institute of Theoretical Chemistry, Jilin University, Changchun 130023, China

S. B. Zhang
State Key Laboratory on Integrated Optoelectronics, College of Electronic Science and Engineering, Jilin University, Changchun 130012, China and Department of Physics, Applied Physics, and Astronomy, Rensselaer Polytechnic Institute, Troy, New York 12180

(Received 8 December 2008; accepted 23 March 2009; published 28 May 2009)

First-principles calculations show unexpectedly large binding (0.7 eV) between positive H^+ at oxygen antibonding site (AB_O) and Ca, which replaces isovalent Zn in ZnO. It is explained by a large spatial undulation of the host charge and the change in the charge due to Ca replacement of the Zn. Our findings are consistent with a number of infrared measurements. © *2009 American Vacuum Society.* [DOI: 10.1116/1.3119679]

I. INTRODUCTION

ZnO is a potential electronic material for next-generation blue optoelectronic applications. However, due to the lack of good quality *p*-type materials, fabrication of ZnO-based optoelectronic devices is still not possible. Much effort has been made both experimentally and theoretically trying to explain the *p*-type doping difficulty. Hydrogen may be a killer as first proposed by Van de Walle[1] in 2000. Hydrogen is a very common impurity in semiconductors because it is abundant in air and is widely used in various growth techniques. Hydrogen is also amphoteric: in *p*-type semiconductors, it acts as a donor, but in *n*-type semiconductors, it acts as an acceptor. In other words, it is always opposite to the prevailing conductivity of the host. However, hydrogen is very special in ZnO. It prefers to form a strong O–H bond with lattice O and acts exclusively as a donor, H^+.[1,2] Therefore, H in ZnO has attracted a lot of attention.[3–11]

Despite the initial suggestion, the most stable configuration of hydrogen in ZnO is still controversial. Independent predictions by different groups[12,13] showed consistently that bond center $BC_\parallel$ site [see Fig. 1(a)] is the most stable configuration with formation energy less than any other sites by at least 0.2 eV. Here, we use ∥ and ⊥ to denote the orientation of the O–H bond with respect to the *c*-axis of ZnO. However, experimental observations deviate from each other: McCluskey *et al.*[6] observed an IR peak at 3326 cm^{-1} in samples provided by Cermet, while Lavrov *et al.*[12] observed a different peak at 3611 cm^{-1} in samples by EaglePicher. Polarized IR showed that the 3326 cm^{-1} peak is associated with an oscillator oriented at 112° angle with respect to the *c*-axis, whereas the 3611 cm^{-1} peak is parallel to the *c*-axis. Later study by Shi *et al.*[7] on both samples showed that the Cermet samples have a strong 3326 cm^{-1} peak and a weak 3611 cm^{-1} peak, but the EaglePicher samples have exactly the opposite. This indicates that there exist two forms of O–H in these samples. Furthermore, the splitting $3611-3326=285$ cm^{-1} is comparable to the calculated splitting between the *BC* site and the *AB* site adjacent to oxygen (AB_O), the 3611 cm^{-1} peak has been assigned to $BC_\parallel$, whereas the 3326 cm^{-1} peak to $AB_{O\perp}$.[13] The dominance of the $AB_{O\perp}$ site in the Cermet samples contradicts with theory as a 0.2 eV difference is considerably larger than the thermal energy at the experimental temperature of 4 K.

Recently, McCluskey and Jokela,[14] by using delayed gamma neutron activation analysis and secondary ion mass spectrometry, found that the Cermet samples contain considerable amount of Ca, whereas the EaglePicher samples do not. This raises an important question as to whether the unintentional impurity, although isovalent to zinc, can cause size switch in some unexpected way.

In this study, we show that Ca has strong Coulomb binding with H^+ in the $AB_{O\perp}$ site despite the fact that Ca is isovalent to Zn. Our finding is consistent with hydrogen in the Cermet samples, i.e., the 3326 cm^{-1} IR peak dominates with the oscillator aligned 112° from the *c*-axis. A new binding mechanism based on charge transfer is proposed to explain the unexpected strong binding.[15]

II. METHOD

Our calculations use first-principles density functional theory[16] within the local density approximation and the projector augmented wave method,[17,18] as implemented in the VASP code.[19,20] Zn 3*d* states are treated as the valence states. The cutoff energy for the plane wave expansion is 400 eV.

[a)] Electronic mail: limaojlu@gmail.com

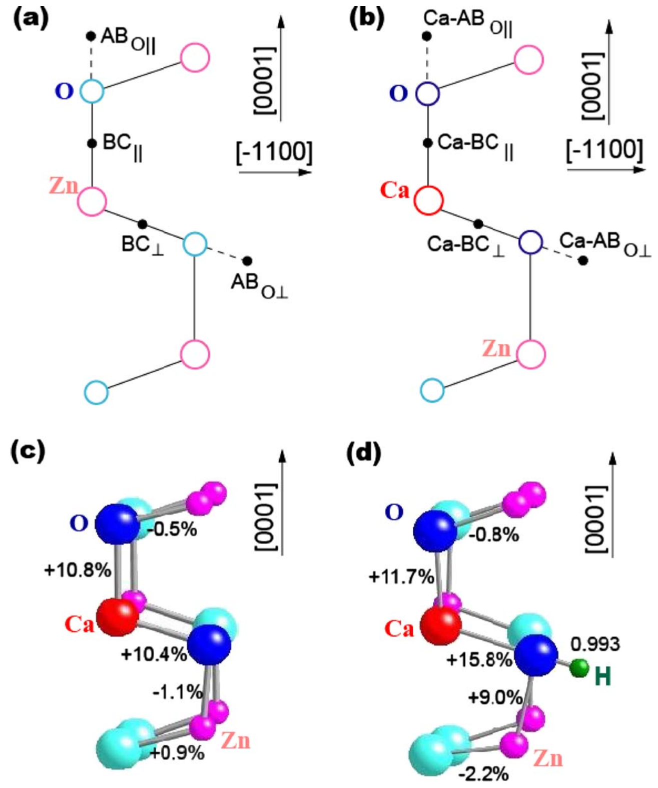

FIG. 1. (Color online) (a) and (b) are schematics of the four H^+ sites in a (11–20) plane in the Ca-free ZnO and near a Ca impurity. (c) and (d) are the calculated atomic relaxations for Ca and Ca–H^+ at the Ca-$AB_{O\perp}$ site, respectively. Oxygen atoms adjacent to the Ca are marked by darker blue.

The calculated equilibrium lattice constant of ZnO is only 1.4% shorter than experiment, and the calculated heat of formation of 3.51 eV agrees with the experimental value of 3.60 eV. We use 48- and 96-atom wurtzite supercells to study the Ca–H pair with the Monkhorst–Pack *k*-point mesh for the Brillouin zone integration ($3\times3\times2$ for 48-atom cell and $2\times2\times2$ for 96-atom cell). Unless noted otherwise, the numerical values presented are for the 96-atom cell calculations. For charged defect, we use the jellium background approximation. All the atoms are relaxed to their equilibrium positions. To calculate the O–H frequencies, we employ the approach in Ref. 13 to include anharmonic effects. For free H_2O molecule, this yields a symmetric stretch frequency of 3540 cm^{-1}, which is lower than experiment[21] by $\omega_{\text{ER}} = 117\ \text{cm}^{-1}$ (an error of $\sim 3\%$). To correct for such a systematic error, we add ω_{ER} to all the calculated frequencies before comparing them with experiments.

III. RESULTS AND DISCUSSION

Figure 1 shows the H-related atomic configurations with and without the Ca. In agreement with previous calculations, we also find that the $BC_{\|}$ site is the most stable configuration in Ca-free ZnO. Hence, we take the $BC_{\|}$ site as the energy reference to define our formation energies,

$$\Delta E = E_{\text{tot}}(\text{Ca-H}^+) + E_{\text{tot}}(\text{bulk}) - E_{\text{tot}}(\text{Ca}_{\text{Zn}}) - E_{\text{tot}}(BC_{\|}), \tag{1}$$

where $E_{\text{tot}}(\alpha)$ is the total energy of a supercell containing the impurity α. In a way, ΔE is the energy required to transfer a $BC_{\|}$ site H^+ from Ca-free ZnO to a Ca-related site in Ca-containing ZnO. A negative ΔE implies that H^+ prefers to go to Ca, whereas a positive ΔE implies that H^+ does not prefer to go, or in other words, the Ca–H pair is only metastable.

Table I shows the calculated formation energy and the O–H distance for Ca-free and Ca-containing ZnO. From the table, we can see that (1) the $AB_{O\perp}$ site next to a Ca is the most stable configuration. This is consistent with experiments on the Cermet samples. (2) Surprisingly, at the Ca-$AB_{O\perp}$ site, the Ca atom and H^+ ion have a strong binding ($0.5+0.2=0.7$ eV, which is almost comparable to the oppositely charged donor and acceptor pairs). Our calculation shows that both substitutional Ca and interstitial H^+ cause outward relaxations to the surrounding Zn and O atoms. Thus, the strong binding here cannot be strain related. If it is neither Coulomb (for opposite charge) nor lattice strain, we need a new mechanism to explain our results.

First of all, we note that, based on the Pauling scale, the electronegativities of Ca, Zn, and O are $\chi^{\text{Ca}}=1.00$, $\chi^{\text{Zn}}=1.65$, and $\chi^{\text{O}}=3.44$, respectively, and ZnO is an ionic semi-

TABLE I. Calculated hydrogen formation energy (relative to H on the $BC_{\|}$ site in the Ca-free ZnO) and O–H bond lengths. Highlighted rows are for the respective ground-state configurations without and with Ca.

	ΔE (eV)		$d_{\text{O-H}}$ (Å)	
Site	96-atom supercell	48-atom supercell	96-atom supercell	48-atom supercell
$BC_{\|}$	**0.00**	**0.00**	**0.985**	**0.986**
$BC_{\perp}$	0.14	0.16	0.985	0.988
$AB_{O\|}$	0.19	0.18	1.001	1.010
$AB_{O\perp}$	0.15	0.17	1.004	1.005
Ca-$BC_{\|}$	0.54	0.65	0.967	0.971
Ca-$BC_{\perp}$	0.38	0.69	0.979	0.964
Ca-$AB_{O\|}$	−0.29	−0.33	0.995	1.002
Ca-$AB_{O\perp}$	**−0.49**	**−0.72**	**0.993**	**1.029**

TABLE II. Calculated hydrogen stretching modes in cm^{-1} for the $BC_{\parallel}$ and $AB_{O\perp}$ sites without and with Ca and compared to those in experiments. For the calculations, the harmonic frequencies and the anharmonic contributions are also shown. ω_{ER} (117 cm^{-1}) is the systematic error of the calculated O–H vibration frequencies (see text for detail).

	Present			
Site	ω_0	$\Delta\omega$	$\omega=\omega_0+\Delta\omega+\omega_{ER}$	Measured ω
$BC_{\parallel}$	3618	−314	3421	3611[a]
$AB_{O\perp}$	3318	−326	3109	
Ca-$BC_{\parallel}$	4022	−205	3934	
Ca-$AB_{O\perp}$	3443	−353	3207	3326[b]

[a] Reference 12.

[b] Reference 6.

conductor with O being the negative charge center and Zn being the positive charge center. Thus, qualitatively speaking, Ca has a stronger tendency to transfer electron to its neighboring O atoms than Zn. In other words, O atoms neighboring a Ca will be more negatively charged than any other host O atoms. A more negatively charged O ion will bind the positively charged H^+ ion more strongly. This makes the Ca-$AB_{O\perp}$ site most stable. Conversely, a more positively charged Ca ion will repel more of the positively charged H^+ than any host Zn ion does. This makes the Ca-$BC_{\parallel}$ sites least stable.

To further our qualitative discussion above, we employ a Bader analysis.[22,23] Our calculations show that in bulk ZnO, each Zn atom donates 1.13 electrons to the neighboring O atoms. In other words, Zn can be considered as a positive center with $q=+1.13e$, whereas O can be considered as a negative center with $q=-1.13e$. This explains why an H^+ prefers to stay close to the O instead of the Zn. Bader analysis on Ca_{Zn} further shows that Ca donates $1.42e$, which is $0.29e$ more than that of Zn. The extra donation is almost equally distributed among the four O nearest neighbors: $0.06e$ to the O atom in the [0001] direction and $0.07e$ to each of the remaining three O atoms in the perpendicular directions. Thus, charge transfer from Ca to its neighboring O atoms is clearly demonstrated.

Next, we need to determine with the method in Ref. 13 if the new configurations would affect the O–H stretching frequencies and the results are shown in Table II. Although the absolute values here differ from experiments by 100–200 cm^{-1}, we find that the difference between the two experimental modes (3611 cm^{-1}–3326 cm^{-1}=285 cm^{-1}) is in reasonable agreement with that between the Ca-free $BC_{\parallel}$ site and Ca-$AB_{O\perp}$ site in the calculation (3421 cm^{-1}–3207 cm^{-1}=214 cm^{-1}). Our calculated Ca-$AB_{O\perp}$ oscillator is oriented 107° away from the *c*-axis, which is consistent with the experiment on the Cermet samples (with a 112° angle), whereas our calculated $BC_{\parallel}$ oscillator is along the *c*-axis, which is also consistent with experiments on the EaglePicher samples.

IV. CONCLUSION

First-principles calculations reveal that the isovalent Ca_{Zn} in ZnO has an unexpected strong Coulomb binding with H^+ ion on the Ca-$AB_{O\perp}$ site. Our finding is consistent with recent experiments and may explain the controversies on the measurements on the Cermet samples. The unexpected binding between Ca and H^+ is explained by a new charge transfer mechanism, which could be universal to ionic solids but absent in covalent materials.

ACKNOWLEDGMENTS

This work was supported by NSFC (Contract No. 60525412), U.S. DOE/BES (Contract No. DE-AC36-99GO10337), JLU (start-up fund), CHE (CHE-RES-RG program), and AOARD/AFOSR (Contract No. FA4869-08-1-4007). The authors would also like to thank D. J. West, Z. G. Chen, X. Meng, and H. Wang for helpful discussions and D. Han, Q. D. Chen, H. Yang, and L. Chen for the technical support.

[1] C. G. Van de Walle, Phys. Rev. Lett. **85**, 1012 (2000).
[2] C. G. Van de Walle and J. Neugebauer, Nature (London) **423**, 626 (2003).
[3] K. Ip, M. E. Overberg, Y. W. Heo, D. P. Norton, S. J. Pearton, C. E. Stutz, B. Luo, and F. Ren, Appl. Phys. Lett. **82**, 385 (2003).
[4] S. J. Jokela and M. D. McCluskey, Phys. Rev. B **72**, 113201 (2005).
[5] E. V. Lavrov and J. Weber, Phys. Rev. B **73**, 035208 (2006).
[6] M. D. McCluskey, S. J. Jokela, K. K. Zhuravlev, P. J. Simpson, and K. G. Lynn, Appl. Phys. Lett. **81**, 3807 (2002).
[7] G. A. Shi, M. Stavola, S. J. Pearton, M. Thieme, E. V. Lavrov, and J. Weber, Phys. Rev. B **72**, 195211 (2005).
[8] K. Shimomura, K. Nishiyama, and R. Kadono, Phys. Rev. Lett. **89**, 255505 (2002).
[9] S. F. J. Cox *et al.*, Phys. Rev. Lett. **86**, 2601 (2001).
[10] C. H. Seager and S. M. Myers, J. Appl. Phys. **94**, 2888 (2003).
[11] M. D. McCluskey and S. J. Jokela, *Proceedings of the NATO Advanced Workshop on Zinc Oxide*, NATO Advanced Studies Institute, Series II: Mathematics, Physics, and Chemistry, edited by N. Nickel and E. Terukov (Springer, Dordrecht, 2005), Vol. 194, p. 125.
[12] E. V. Lavrov, J. Weber, F. Börrnert, C. G. Van de Walle, and R. Helbig, Phys. Rev. B **66**, 165205 (2002).
[13] S. Limpijumnong and S. B. Zhang, Appl. Phys. Lett. **86**, 151910 (2005).
[14] M. D. McCluskey and S. J. Jokela, Physica B **401–402**, 355 (2007).
[15] X. B. Li, S. Limpijumnong, W. Q. Tian, H. B. Sun, and S. B. Zhang, Phys. Rev. B **78**, 113203 (2008).
[16] W. Kohn and L. J. Sham, Phys. Rev. **140**, A1133 (1965).
[17] P. E. Blöchl, Phys. Rev. B **50**, 17953 (1994).
[18] G. Kresse and D. Joubert, Phys. Rev. B **59**, 1758 (1999).
[19] G. Kresse and J. Furthmüller, Phys. Rev. B **54**, 11169 (1996).
[20] G. Kresse and J. Furthmuller, Comput. Mater. Sci. **6**, 15 (1996).
[21] E. McCartney, *Absorption and Emission by Atmospheric Gases: The Physical Processes* (Wiley, New York, 1983).
[22] R. F. W. Bader, *Atoms in Molecules: A Quantum Theory* (Oxford University Press, New York, 1994).
[23] G. Henkelman, A. Arnaldsson, and H. Jonsson, Comput. Mater. Sci. **36**, 354 (2006).